Design & Modeling of a MEMS Contact-mode Piezoresistive Detector for Pull-in Acceleration Sensing

Author: Bou Sing Hau B.Sc

Student Number: 1192353

Daily Supervisor: Vijay Rajaraman B.E., M.Sc.

External Advisor : Prof. Dr. L.A. Rocha

University of Minho, Guimaraes, Portugal

Project Professor: Prof. Dr. P.J. French

Thesis Committee:

Prof.Dr.Ir. R. Dekker

Dr.Ir. A. Bossche

July 11, 2011

Abstract

Recently a new kind of accelerometer was developed. The accelerometer uses the pull-in time to measure the accelerations. However most of the applied measurement techniques for this kind of accelerometers had shown some drawbacks in the working process. So in this dissertation a new measurement method is introduced based on piezoresistivity to overcome some of the issues. The new measurement method made use of the piezoresistive contact-mode detectors. In this project the detectors were investigated for the realization of pull-in time accelerometers. The working principle of this measurement technique was as follows, when pull-in occurs, the piezoresistive contact-mode detector senses the movement and a signal is created to signify the impact event. The contact method approach is introduced and explained in detail in the thesis along with simulated and experimental data from fabricated microdevices. The sensitivity of the fabricated detector was found to be 0.1mV/nm.

Acknowledgements

First of all, I want to thank daily supervisor Vijay Rajaraman, for helping me out when I encounter some problems and for arranging the things that was needed for my project and a lot more.

Secondly, I want to thank my external advisor Prof. L.A. Rocha, for sharing his ideas and of course helping me a lot during the project. He was a very busy person and still he made some time free to meet me regularly, I am really grateful to him for that. I also want to thank Rosana Dias for sharing her ideas with me and gave me comments.

Thirdly, I want to thank my project professor Prof. P.J. French for his help and support and also for arranging the materials that I needed to work on the project.

I also want to thank Prof. Heng Yang for his help and his comments and sharing his experience with me.

Last, but certainly not least I want to thank my parents, my brother, my sister and especially my girlfriend Joy Qiao for supporting me and understanding my difficulties during the project.

This MSc thesis work is a result of collaborative scientific work and exchange of ideas with my daily supervisor, Vijayekumar Rajaraman, at the Delft University of Technology (TU Delft), The Netherlands.

Table of Contents

Table of Figures

1 Introduction

Accelerometer is a device used for measuring linear acceleration, tilt angles or vibration of an object. These devices are used in different applications (Figure 1.2) such as automotive, GPS, oil-exploration, earthquake prediction, human motion monitoring, medical equipment, gaming, robotics, data entry, mobile phones etc. For various kind of application the specification requirement are also different. For example, in the gaming industry the precision is less important than for medical or military applications. Thus, since the first micromachined silicon accelerometer was developed at the Stanford Integrated Circuit Laboratory for biomedical applications in 1978 [1], many micro machined silicon accelerometers have been developed with different kind of operating principles and structures. The various operating principles have their own advantages over other principles and thus diverse application requirements can be fulfilled.

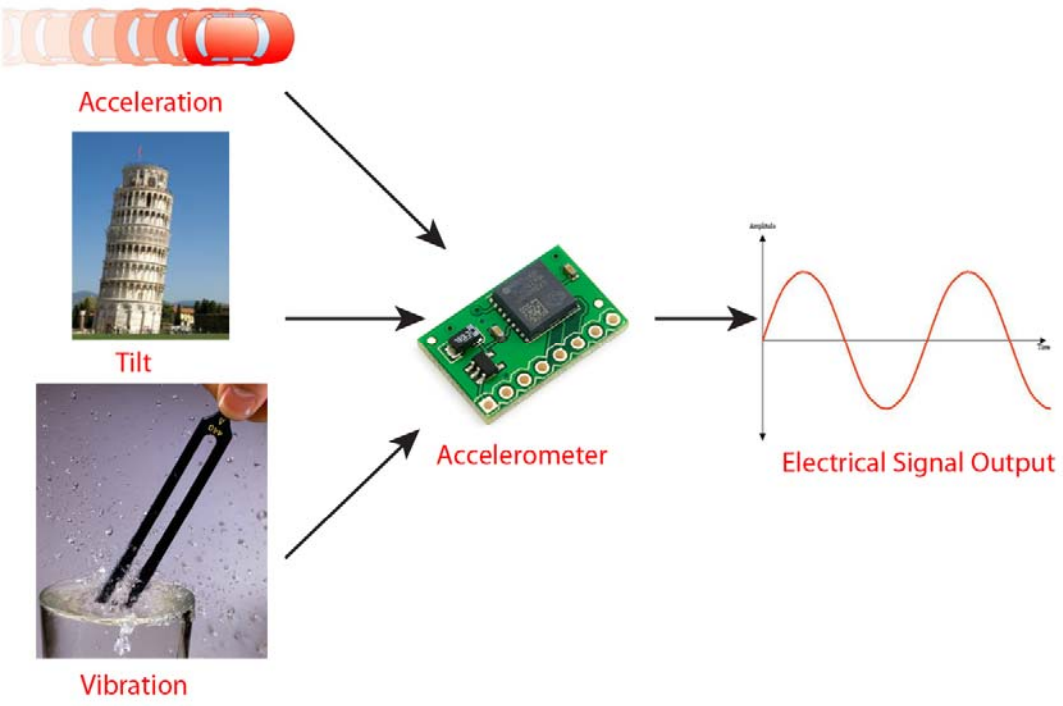

Figure 1.1 The Functionality of the Accelerometer

High precision and cheap accelerometers are increasingly needed. Reducing prices of accelerometers is possible by using microtechnologies. As one might know the more identical product is made the cheaper the cost will be. In [2] it has been reported that batch fabrication of an accelerometer using silicon IC technology is possible with some good performance. So it can be concluded that batch fabricated MEMS micromachined accelerometers are the solution for this problem.

Figure 1.2 Applications of Accelerometer

The working principle of a conventional micro machined accelerometer is as follows. The accelerometer contains a proof mass which is attached to some springs that in its turn connected to the frame (Figure 1.3). As the mass inclines due to acceleration, the spring will bend and thus stress will be generated. By converting the stress on the bending spot (the stress on these spots are the largest) to resistance changes using piezoresistors an electrical output voltage can be generated, which corresponds to the inertial acceleration the device undergoes.

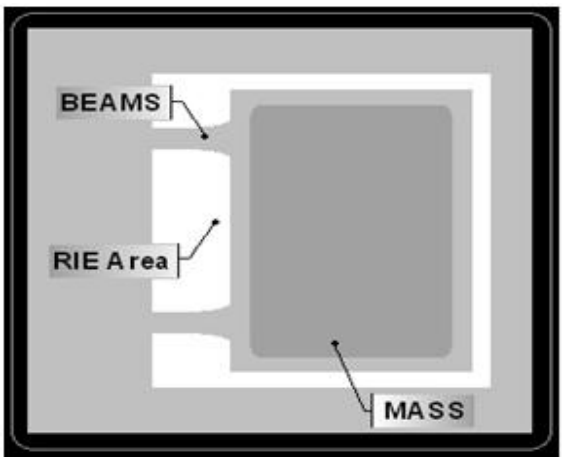

Figure 1.3 Top View of a Conventional Piezoresistive Accelerometer [3]

1.1 Overview of Accelerometer Types

Accelerometers can be classified by their measurement technique.

- Capacitive accelerometers: The accelerometer converts the inertial acceleration into capacitance changes and by measuring the capacitance change the acceleration can be extracted from the measurement. Usually these accelerometers contain beam shaped structures to generate the capacitance. [4]
- Piezoelectric accelerometers: The device turns the inertial acceleration into stress due to bending and subsequently converts the stress into a signal in the electrical domain, which represents the acceleration. The most common usage of this transduction is by putting piezoelectric material on the springs that connect the mass to the frame. [5]
- Piezoresistive accelerometers: The working principle of this type is very similar to the piezoelectric accelerometers. First the device converts the inertial acceleration to stress due to bending and next the stress is turned into a signal in the electrical domain due to the resistive changes. Usually this type of accelerometer contains beam structures, which are sensitive for force and thus generates stress. [6,7]
- Vibrating Beam accelerometers: For the accelerometer that is introduced in [8]. When acceleration is applied. The mass of the accelerometer, which is attached by hinges, rotates about the axis of the flexure hinges and generate a force to the silicon resonator which in turn changes the resonant frequency. The amount of changes in the resonance frequency depends on the magnitude and direction of the applied acceleration. So by measuring the resonant frequency the acceleration can be extracted
- Hall Effect accelerometers: This accelerometer uses an object that generates a magnetic field to measure the acceleration or actually the displacement. Due to the magnetic field the Hall sensor can be used to detect by how much the object has moved and thus the acceleration of the object. [9]
- Magnetoresistive accelerometer: It has been reported that by using a balanced Wheatstone bridge circuits in combination with an elastic magnet, the acceleration can be measured. In the situation where no acceleration is applied the output is balanced, however when acceleration is added to the system the balance is disturbed and the acceleration can be measured.[10]
- Heat transfer accelerometer: This kind of accelerometer makes use of the heat to measure the acceleration. This accelerometer makes use of a heater and two equally distanced thermal sensor. When there is no acceleration the thermal sensor are producing identical electrical outputs, however when acceleration is applied the balance of the heat transfer from the heater to the two sensors will be disturbed and thus the acceleration can be derived from this measurement.[11]
  Another type of heat transfer accelerometer is mentioned in [12]. The basic accelerometer contains a mass attached to four springs and a heat source and thermopiles. The thermopiles are used to measure the temperature of the heat source. The mass with a heat sink attached is hanging above the heat source. The heat flow depends on the distance between the heat source and the mass. When accelerated the distance will be reduced and the heat flow will increased and the temperature of the heat source will be reduced and the acceleration can be extracted.
- Tunnelling effect accelerometer: The operating principle of this accelerometer is as follows: first the tip of the proof mass is brought close to the counter electrode by using

the electrostatic force generated by the bottom deflection electrode. A tunnelling current is then established and it should remain constant as long as the device is in a stable state. When there is some disturbance like acceleration then the readout circuit will respond to the change of the tunnelling current and adjust the deflection voltage to move the proof mass back to its stable state. The deflection voltage corresponds to the applied acceleration. [13,14]

- Interferometric accelerometer: This accelerometer makes use of a light source and some light detectors. Usually when the fingers which are attached to the proof mass are illuminated with a coherent light, a diffraction pattern is reflected. However when the mass has moved due to acceleration the intensity of the diffracted beams are changed and thus the acceleration can be extracted.[15]

The capacitive, piezoelectric and piezoresistive are the conventional methods and thus they are the most developed techniques used in MEMS based accelerometers. In this project the piezoresistive transduction method is used to detect the acceleration.

1.2 Motivation & Objectives

Micromachined accelerometers have been widely applied in different field of applications. While traditional piezoresistive, piezoelectric and capacitive transduction approaches have been used, in [16] it was found that the acceleration can also be measured using the transition time of the proof mass for one complete cycle. Initially, the transition time detection method was based on the contact occurring between the proof-mass and a hard stopper [16], followed by another method based on the FET-based capacitive sensing [17]. Recently an improved sensing approach, employing contactless capacitive sensing was reported [18]. However the first two methods suffer from poor contact and sensitivity and face reliability issues while the last method consumes a large area. To overcome some of these issues piezoresistive sensing is chosen to be used in this project. The main advantages of using piezoresistive sensing are:

- Simple read-out circuitry
- Good linearity
- Scalability
- Compactness

Since the predecessors are suffering from different kind of problems, the main objective of this thesis work is to design a novel detection method to overcome some of the problems with comparable performance, based on piezoresistivity.

1.3 Thesis Organization

The thesis is organized into six chapters. The first chapter gives an introduction to the reader about the thesis while the second chapter gives an overview of the background theories that are used in this work. In chapter 3 the design of the system is explained. This includes the analytical and numerical analyses done in COMSOL and Simulink. Chapter 4 reports the technology used to fabricate the devices and chapter 5 explains the measurement setup and the measurement details including results. Finally, in the last chapter some conclusions are drawn and recommendations for future work are given.

2 Theoretical Background

This chapter introduces the underlying theories supporting this thesis. The involved mechanics as well as the electrical aspects are explained here. At the end of this chapter the operation principle of the time base accelerometer is explained.

2.1 Mechanics

Spring Constant

Spring constant is a very important parameter for an accelerometer. Spring constant is defined as the force that is needed for the proof mass (in this case) to achieve an unit displacement. This prarameter also defines the performance of the accelerometer. The basic spring constant can be expressed as:

$$k = -\frac{F_m}{d} \tag{2.1}$$

where F the applied force and d the deflection. For a beam that is fixed at one end the spring constant can be calculated using a derived equation from beam deflection theory [19]. The deflection depends on which direction the force is applied, resulting in different governing equations. These are given by Eqs.(2.2),(2.3)&(2.4).

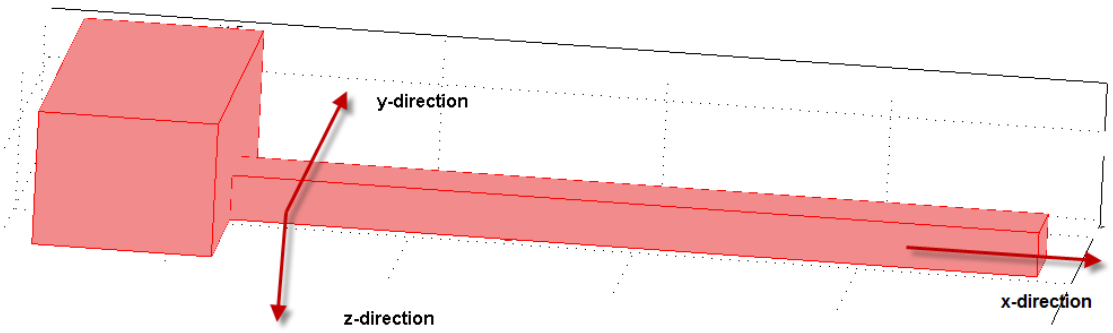

Figure 2.1 Beam Fixed on One End

$$k_x = \frac{Etw}{l} \tag{2.2}$$

$$k_y = \frac{Etw^3}{4l^3} \tag{2.3}$$

$$k_z = \frac{Et^3 w}{4l^3} \tag{2.4}$$

Where E is the Young's modulus, t is the thickness, w is the width of the beam and l is the length of the beam. If there is a mass attached to the spring, the angular frequency can be calculated using the spring constant and is defined as:

$$\omega_0 = \sqrt{\frac{k}{m}} \tag{2.5}$$

where k is the spring constant and m is the mass.

Stress

Mechanical stress can be used for generating a signal using piezoresistive and piezoelectric transduction techniques. The force-stress relation is given as

$$\sigma = \frac{F}{A} \tag{2.6}$$

Where σ is the stress, F is the force and A is the area where the force is exerted on. In the case of using the cantilever shown in Fig.2.1, the maximum stress will occur at the clamping point and the force moment is given as

$$M = F(L - x) \Rightarrow M_{\max} = FL \tag{2.7}$$

where L is length of the beam and x is the distance from the end of the beam where the force is exerted. The maximum stress is given as

$$\sigma_{\max} = \frac{M_{\max}}{I} y = \frac{FL}{I} y = \frac{12FL}{wt^3} \frac{h}{2} = \frac{6FL}{wt^2} \tag{2.8}$$

Where w is the width of the beam and t is the height of the beam. Assuming that the force is a point force, where y is the distance from the edge to the neutral axis and I the moment of inertia ($\frac{wt^3}{12}$ for cantilever).

2.2 Electrical Aspects

Capacitance

Capacitance is a multifunctional parameter that can be used for sensing and/or actuation.

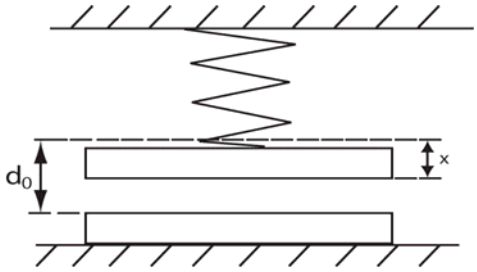

Figure 2.2 Parallel Plate Capacitor

Figure 2.2 shows a parallel plate capacitor. If a potential is applied over the capacitor the movable plate that is attached to the spring will move according to the given potential and the capacitance changes. The capacitance is given by:

$$C = \frac{A\varepsilon\varepsilon_0}{d_0 - x} \tag{2.9}$$

where A is the area of the electrodes, $\varepsilon_0 = 8.854 \times 10^{-12} F/m$ is the permittivity of vacuum, ε_r the relative permittivity of the medium between the electrodes, d_0 is the initial gap between the electrodes and x is the displacement that one of the plate has undergone. Using the capacitance changes, the parallel plates can be used to sense by how much the plate has moved compared to the initial position. The electrostatic force can be calculated as:

$$F_e = \frac{1}{2}\frac{A\varepsilon\varepsilon_0}{(d_0 - x)^2}V^2 \tag{2.10}$$

This equation shows that the parallel plate capacitor can be used as actuator. By changing the applied potential V the force can be controlled.

Piezoresistor

Resistivity

To understand how resistances in silicon work, several concepts need to be introduced. The resistance depends on the doping profile and so the conductivity. The conductivity is given by [20]

$$\sigma = ne\mu_n + pe\mu_p \tag{2.11}$$

where n, p are the electrons and holes concentration, e is the elementary charge and μ_n, μ_p are the mobility of the electrons and holes. The resistivity is inversely proportional to conductivity and is given by

$$\rho = \frac{1}{\sigma} = \frac{1}{ne\mu_n + pe\mu_p} \tag{2.12}$$

The electrical resistance can be calculated as:

$$R = \rho \frac{l}{A} \tag{2.13}$$

where A is the cross-sectional area of the resistor. From these equations it can be seen that the electrical resistance depends on both the dimensions of the resistor and the material properties.

Gauge Factor

The gauge factor is usually used to define the sensitivity of the piezoresistors that use the stress as the measure parameter. Gauge factor is also defined as the change in resistance per unit change of the strain. Usually p-type poly-silicon or p-type mono-crystalline silicon is used for the piezoresistors since the sensitivity is higher than the n-type silicon. [21, 22, 23] suggests that the maximum gauge factor for p-type poly-silicon occurs at a doping of $2\times10^{19} cm^3$ and so, if p-type poly-silicon is used the resistors should be doped with $2\times10^{19} cm^3$ in order to get a longitudinal gauge factor as high as 40. If mono-crystalline silicon is used for the piezoresistor, the p-type silicon gauge factor can be calculated. Gauge factor is in general defined as:

$$GF = \frac{\Delta R}{R\varepsilon} \tag{2.14}$$

where $\frac{\Delta R}{R}$ is the resistance change and ε is the strain. Strain is defined as

$$\varepsilon = \frac{\sigma}{E} \tag{2.15}$$

where σ is the stress and E is the Young's modulus. For p-type silicon the longitudinal piezoresistive coefficient of the resistor aligned along the [110] direction in the (001) plane is given by [24]

$$\pi_{l,110} = \frac{1}{2}\left(\pi_{11} + \pi_{12} + \pi_{44}\right) \tag{2.16}$$

and the resistivity changes are calculated as:

$$\frac{\Delta\rho}{\rho} = \pi_l \sigma_l + \pi_t \sigma_t \tag{2.17}$$

Since the transverse stresses are small [25] it can be neglected and Eq.(2.17) can be rewritten as

$$\frac{\Delta\rho}{\rho} = \pi_l \sigma_l \tag{2.18}$$

and [26]

$$\frac{\Delta\rho}{\rho} \approx \frac{\Delta R}{R} \tag{2.19}$$

So using Eqs.(2.14)-(2.19) the gauge factor of p-type piezoresistors can be calculated: $GF = 104.29$ (using [25] $\pi_{11} = 1.8\times10^{-11} Pa^{-1}, \pi_{12} = 2.5\times10^{-11} Pa^{-1}, \pi_{44} = 118.4\times10^{-11} Pa^{-1}$).

2.3 Time Based Accelerometer

A pull-in time accelerometer is based on the pull-in principle. During operation the mass is driven from one stopper (A) to the other stopper (B) and the elapsed time for this operation is the so called pull-in time. The differences in the corresponding pull-in times are proportional to the acceleration [16]. The pull-in time of the system without acceleration is defined as t_0 and the time for moving from stopper A to stopper B t_1 and vice versa t_2. When there is no external applied accelerations $t_0 = t_1 = t_2$ otherwise $t_1 \neq t_2 \neq t_0$.

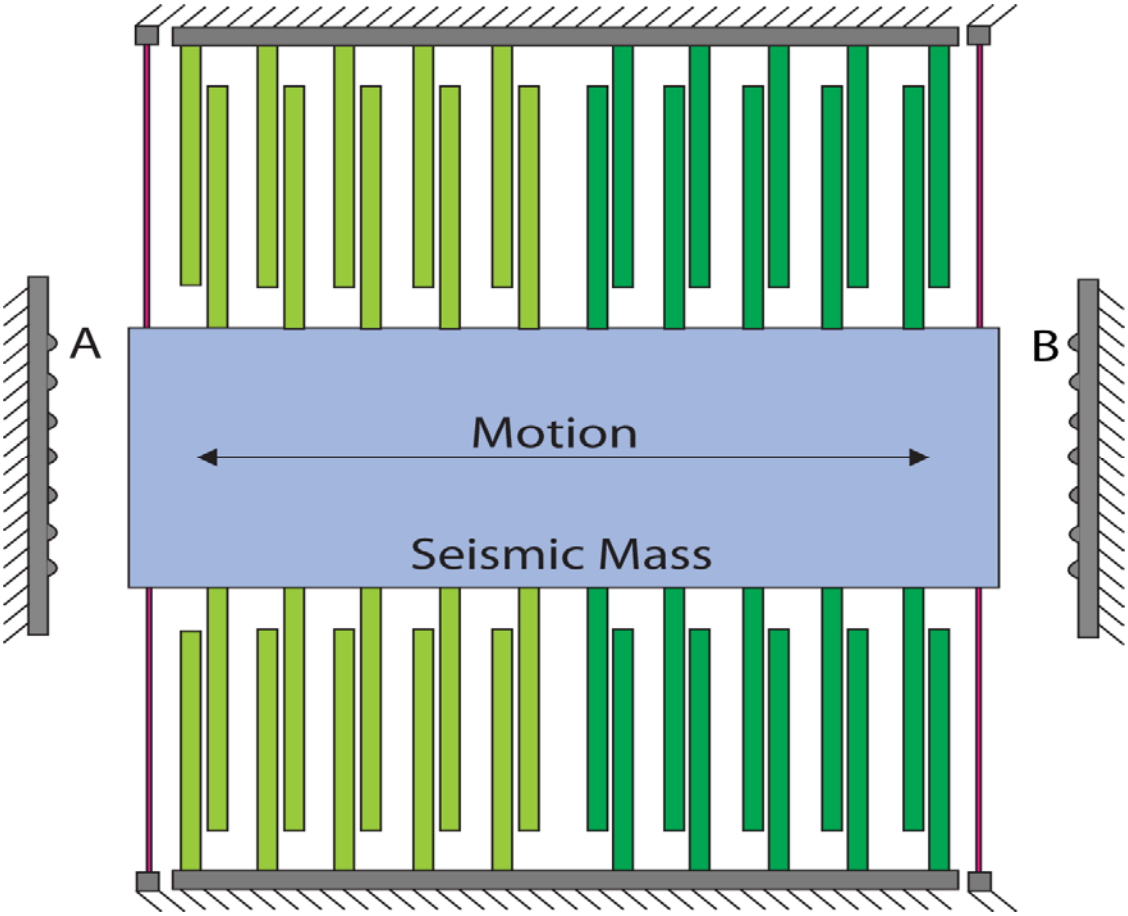

Figure 2.3 Principle of a Pull-in Time Based Accelerometer

Pull-in Principle

The pull-in effect consists of two parallel plates suddenly snapping to each other when subjected to a voltage potential higher than a certain threshold voltage. This event will occur if the system satisfies the conditions. To have a better understanding of this principle within a MEMS system an analytical analysis is performed. The capacitance of the parallel plate capacitor is given in Eq.(2.9). Figure 2.2 shows an electrode attached to a spring that is movable while the other is fixed. When a voltage is applied on the electrodes an electrostatic force is created. The electrostatic force will reduce the gap size between the plates. At small voltages the electrostatic force will be counteracted by the mechanical force $F_m = -kx$, under equilibrium. But once the voltage is increased to a certain value (pull-in voltage) the electrostatic force will overcome the mechanical force and the pull-in event will occur. To estimate the pull-in voltage and the displacement at pull in, the potential energy of the system is introduced as [27]:

$$E = \frac{1}{2}CV^2 - \frac{1}{2}kx^2 = \frac{1}{2}\frac{A\varepsilon\varepsilon_0}{(d_0 - x)}V^2 - \frac{1}{2}kx^2 \tag{2.20}$$

where V is the applied voltage and k the spring constant. The first term is the energy that is due to the capacitor and the voltage source and the second term is the potential energy stored in the spring. The force of the system can be derived by differentiating the total energy to the displacement:

$$F = \frac{\partial E}{\partial x} = \frac{1}{2}\frac{A\varepsilon\varepsilon_0}{(d_0 - x)^2}V^2 - kx \tag{2.21}$$

The system is in equilibrium when the net force is zero, which means that the first term and the second term cancel out each other.

$$F = 0 \Rightarrow \frac{1}{2}\frac{A\varepsilon\varepsilon_0}{(d_0 - x)^2}V^2 = kx \tag{2.22}$$

The system is a second order system with respect to the displacement which means the curve of the net force has a parabolic structure. To derive the stability of any point of the curve the force derivative is used:

$$\frac{\partial F}{\partial x} = 0 = \frac{A\varepsilon\varepsilon_0}{(d_0 - x)^3}V^2 - k \tag{2.23}$$

Substitute Eq.(2.22) in Eq.(2.23) yields:

$$\frac{\partial F}{\partial x} = \frac{2kx}{d_0 - x} - k \tag{2.24}$$

This gives

$$\frac{\partial F}{\partial x} = 0 = \frac{2kx}{d_0 - x} - k \Rightarrow \frac{2kx}{d_0 - x} = k \Rightarrow \frac{2x}{d_0 - x} = 1$$
$$\Rightarrow 2x = d_0 - x \Rightarrow 3x = d_0 \Rightarrow x = \frac{1}{3} d_0 \tag{2.25}$$

The condition for a stable state is mathematically given as:

$$\frac{\partial F}{\partial x} < 0 \Rightarrow x < \frac{1}{3} d_0 \tag{2.26}$$

From Eq.(2.25) it is shown that the turn around point is at one third of the original gap. Eq.(2.26) shows that beyond this point the system becomes unstable which means the pull-in event occurs. To derive the pull-in voltage the displacement in Eq.(2.22) is replaced with $\frac{1}{3} d$ and solving this equation gives:

$$\frac{1}{2} \frac{A\varepsilon\varepsilon_0}{\left(d_0 - \frac{1}{3} d_0\right)^2} V^2 = \frac{1}{3} k d_0 \Rightarrow V = \sqrt{\frac{8kd_0^3}{27 A\varepsilon\varepsilon_0}} \tag{2.27}$$

Eq.(2.27) shows the pull-in voltage which means the pull-in event will occur if the applied voltage is larger than the pull-in voltage.

Pull-in Regions

During a pull-in transition three different regions can be distinguished, the meta-stable region and the stable and unstable regions.

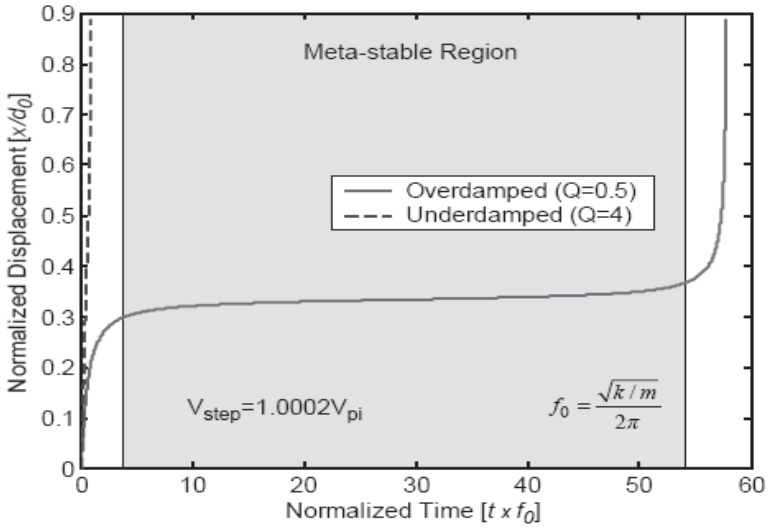

Figure 2.4 Pull-in Motion Characteristic of Overdamped and Underdamped MEMS Devices [4]

Figure 2.4 shows that three regions can be identified in the system. In the first region the system moves fast until it reaches the static pull-in point ($\frac{1}{3}d_0$). Then the system enters the second region which is the metastable region and the third region is the unstable region. It can be seen that while the system is in the meta-stable region it moves slowly. This effect occurs due to the mechanical and the damping forces that counteract the electrostatic force created by the voltage applied to the electrodes. In the meta-stable region the electrostatic force is only slightly higher than the opposing mechanical and damping forces, so the system is moving slowly. During this region the system is very sensitive to external forces since a small force will already destabilize the equilibrium.

To make use of this effect there are conditions that need to meet. First of all the system needs to be overdamped, which means the system has a decent damping force to compensate the electrostatic force. Figure 2.4 shows that when the system is underdamped the total pull-in motion is very fast. Secondly the applied voltage should be slightly greater than the pull-in voltage since the pull-in voltage is the minimum voltage required to initiate a pull-in event.

Operation Principle

In the pull-in accelerometer the on-off principle will be used. The mass is driven by the electrode and will move towards the stopper A, once A is reach or the threshold is met the driving electrode is turned off and the other driving electrode is turned on and pulling the mass towards the opposite direction to stopper B. To reduce errors in the system the initial velocity or rather initial force of the mass should be zero in order to satisfy the assumption that was made while deriving the pull-in distance and the pull-in voltage. So the applied pull-in voltage should have an on time longer than the nominal pull-in time in order to let the system work properly.

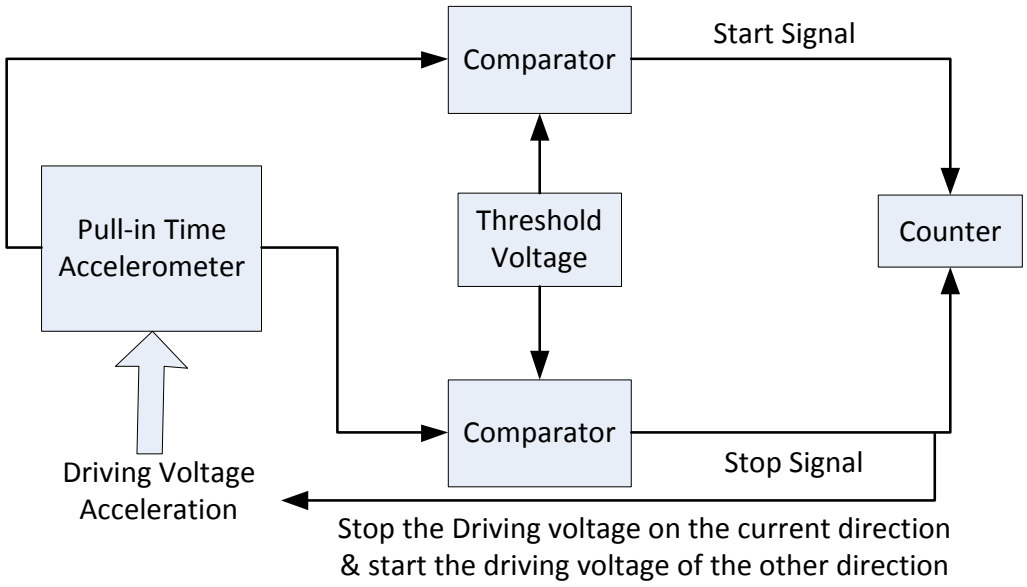

Figure 2.5 Simplified Model of Operation Principle

3 Modelling & System Design

In the previous chapters an introduction to accelerometers was given along with the relevant background knowledge required. In this chapter the system modelling and designs are introduced and explained. To be able to design a detector various considerations need to be investigated in detail. Since a pull-in time accelerometer is used in this work, the pull-in time derivation will be introduced. And the structure of the accelerometer will be shown together with its design parameters. Next the pull-in voltage is calculated. And Simulink models are created to describe the device dynamics. Finally the detector design for the contact method is investigated and the detection for the contactless method is explained.

3.1 Considerations

For a proper accelerometer design, the device behaviour and the transduction mechanism must be clearly understood. This project uses a novel detection method to detect the pull-in time using piezoresistive sensing. The novel detection method uses a flexible stopper: the detector has a sensing function and at the same time the detector will also stop the mass from moving or slow the mass velocity down. Therefore, the detector behaviour can be divided into three stages: when the mass strikes the detector, when the mass pushes the detector and when the mass leaves the detector. During these three stages the mechanics that need to be considered are: how should the collision be detected, how will the detector behave during the collision and what is the behaviour of the detector when the mass leaves.

Collision Detection

Collision between the mass and the flexible detector will be detected due to the stress generated on the detector by the collision. Measuring the stress of the structure allows collision detection. To convert the stress to a parameter which is usable in the electrical domain piezoresistor will be used. Piezoresistors can be realized in silicon by doping specific regions. To make the detector accurate the time delay due to the read-out electronics needs to be accurate if different read-out electronics are used for different sides. However if the read-out electronics used for both sides are the same, the time delay due to read-out electronics can be neglected. Since the delay due to electronics are the same for both sides.

Collision behaviour

An important parameter to consider is the detector behaviour when the mass hits it. Since the mass is driven by the electrodes, which means that it is not a free collision. The mass will more likely press the flexible stopper. This is true unless the voltages on the electrodes are switched off before or during the collision. Since the mass is pressing the flexible detector it is assumed that the force exerting on the mass will be totally transferred to the stopper through the collision area. While the electrostatic force is still exerting on the flexible stopper through the mass, the mass

moves with the compression of the stopper. The electrodes that are attached to the mass are also moved and this means that the gap between the electrodes in the parallel plate structure is smaller again, which generates a greater electrostatic force on the mass that makes it move even further. This behaviour will hold until there is force equilibrium or the electrodes snap to each other. Since the electrostatic force is generated by the capacitive electrodes the force will be increased inversely proportional with the decrease of the gap. This means that force equilibrium does not occur since the counter force, the force generated in the detector and the springs, is increased proportionally with the movement. So the second option needs to be considered. To prevent the snapping between the electrodes, the voltage on the driving electrodes need to be turned off before it snaps completely. However since this is very difficult to achieve another method is considered. By putting fixed hard stoppers behind the detector (Figure 3.1), the electrodes can be prevented from snapping. In the first approach the delay in the sensing mechanism has to be taken into account, because the driving electrode cannot switch off instantly by the output of the read-out electronics. With the latter solution the purpose of using the flexible stopper might on the first glance be nullified. However while the mass collides with the flexible stopper most of the impact is already absorbed which means the damage created on the hard stoppers due to collision is limited.

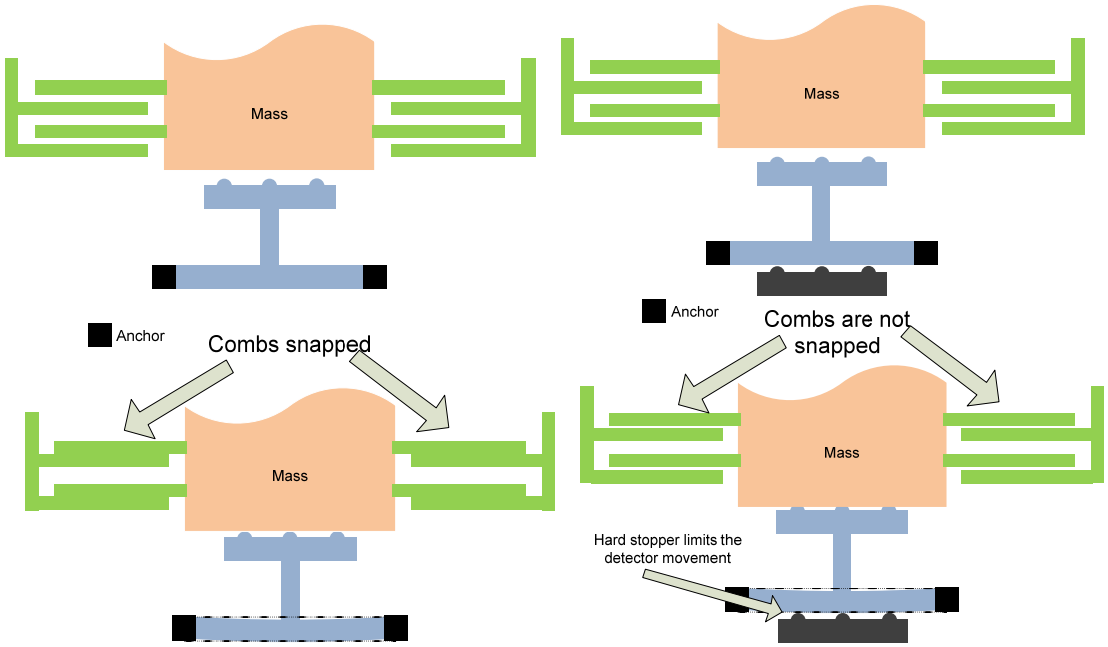

Figure 3.1 Flexible stopper without (left) and with hard stopper (right). If the movement of the flexible stopper is not limited the combs will snap together at the end. If hard stoppers are placed behind the flexible stopper the flexible stopper movement is limited, so the mass cannot move further and the combs will not snap.

After collision behaviour

When the mass leaves the flexible stopper, the stopper is supposed to return to its rest state (settle down) and wait for the next cycle without too many oscillations. This can be done by using an overdamped structure. Due to the overdamped environment the stopper will have a small settling time. So the detector settles before the mass comes back. Another consideration about this occurrence is as follows, will the mass leave the flexible stopper without any initial force.

Because when the mass leaves the flexible stopper, the flexible stopper is bent. This means energy has been stored in the flexible stopper, so when the mass leaves the stopper the mass is being pushed away by the detector. Therefor to not let the detector influence the accelerometer's behaviour, it is required that the mass does not enter its actual cycle with an initial force to minimize the error. If the mass has an initial force then this problem needs to be solved. To fulfil this requirement the accelerometer itself needs to be worked in an overdamped environment where the initial force will be nullified before the actual cycle of mass begins.

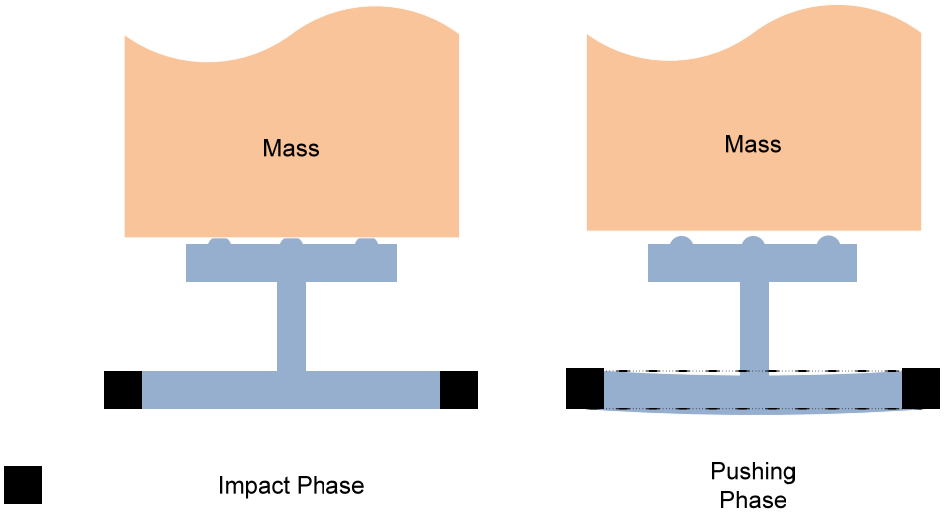

Figure 3.2 Detector Phases

3.2 Analytical Model of the Pull-in Time System

To analyse the system dynamics, an analytical model of the system needs to be derived. In this accelerometer the pull-in time is used to measure the accelerations. Next, the pull-in time derivation will be performed.

Pull-in Time Derivation

The Motion of the seismic mass is governed by the equation (the damped vibration system without external forces)

$$m\ddot{x} + c\dot{x} + kx = 0 \tag{3.1}$$

In this case the motion is influenced by the external forces

$$F_e = \frac{\partial E}{\partial d} \tag{3.2}$$

$$E = \frac{1}{2} C V^2 \tag{3.3}$$

$$C = \frac{A \varepsilon_0 \varepsilon}{d} \tag{3.4}$$

$$\Rightarrow E = \frac{1}{2} \frac{A \varepsilon_0 \varepsilon}{2 d^2} V^2 \tag{3.5}$$

$$F_e = \frac{\partial E}{\partial d} = -\frac{A \varepsilon_0 \varepsilon}{2 d^2} V^2 \tag{3.6}$$

Where A is the area of the plates, ε_0 the permittivity of vacuum, ε the relative permittivity of the medium between the parallel plates, V the applied voltage and d the gap size. Since the gap size can change, the equation can be rewritten as

$$F_e = -\frac{A \varepsilon_0 \varepsilon}{2 \left(d - x \right)^2} V^2 \tag{3.7}$$

where d is the initial gap size and x as the moved distance.

The second force which influences the system is the acceleration force

$$F_a = ma \tag{3.8}$$

putting the equations together gives [16]

$$m\ddot{x} + c\dot{x} + kx = \frac{A \varepsilon_0 \varepsilon}{2 \left(d - x \right)^2} V^2 + ma \tag{3.9}$$

To gain a better understanding of the characteristics, the equation is translated into a dimensionless equation.

$$\frac{d^2}{d\tau^2} \tilde{x} + 2\zeta \frac{d}{d\tau} \tilde{x} + \tilde{x} = \frac{\tilde{F}}{\left(1 - \tilde{x} \right)^2} + \tilde{a} \tag{3.10}$$

To be able to solve this equation analytically the damping is neglected and the equation of motion becomes

$$\frac{d^2}{d\tau^2} \tilde{x} + \tilde{x} = \frac{\tilde{F}}{\left(1 - \tilde{x} \right)^2} + \tilde{a} \tag{3.11}$$

this can again rewritten into

$$\tau = \int_{-\lambda}^{\lambda} \frac{1}{\sqrt{\lambda+\tilde{x}}\sqrt{(\lambda-\tilde{x})+2\tilde{a}+\frac{2\tilde{F}}{(1-\tilde{x})(1+\lambda)}}} d\tilde{x} \tag{3.12}$$

this shows that the pull-in time is proportional to the acceleration.

3.3 Designs

In this dissertation the pull-in time is used as the translation mechanism to measure accelerations. The pull-in time can be affected by the external acceleration or by the applied voltage to the actuators. For high sensitivity a voltage which is slightly higher than the pull-in voltage is used. This is to ensure that the meta-stability occurs [18]. To prove the piezoressitive based pull-in time accelerometer two different designs were included in the project.

To be able to design a detector for the accelerometer, the accelerometer structure needs to be known and understood. The accelerometer structure in Figure 2.3 was used as the base for designing the detectors. The specifications are listed in Table 3.1 [28].

Mass (µg)	0.249
Spring constant (N/m)	3.3295
Resonance frequency (Hz)	582
Zero-displacement gap (µm)	2.25
Zero-displacement capacitance (pF)	2.53
Damper length (µm)	500
Number of comb fingers (dampers)	4 × 29
Number of drive comb fingers	4 × 6
Thickness comb finger (m)	25×10^{-6}
Length comb finger (m)	500×10^{-6}
Permittivity (F/m)	8.8546×10^{-12}
Gap size 1 (m)	2.25×10^{-6}
Gap size 2 (m)	20×10^{-6}
Damping coefficient (@1/3 gap) (mN.s/m)	2.6
Quality factor	0.35
Acceleration noise (µg/√Hz)	2.69
Sensitivity (µs/µg)	0.12
Pull-in voltage (V)	2.92
Nominal Pull-in time (ms)	18.5
2g displacement (µm)	1.462

Table 3.1 Accelerometer Specifications

3.3.1 Pull-in Voltage

In the system the comb fingers are attracted on 2 sides. By design the gap in the direction of interest is smaller and is defined as $d_{01} = 2.25\times10^{-6}$ and the other side as dimensions, $d_{02} = 20\times10^{-6}$. From previous calculations it has been shown that a parallel plate system will be

stable until $\frac{1}{3}d_0$ if only the direction of interest is taken into account. For the situation in which both sides are taken into account, compensation is needed to remain stable at the same position.

The stability equation is given as

$$\frac{AEV^2}{2\left(d_{01}-x\right)^2}-\frac{AEV^2}{2\left(d_{02}+x\right)^2}-kx=0 \tag{3.13}$$

So filling in the parameter values gives (considering that $x_{pi}=\frac{1}{3}d_0$)

$$\frac{2*6*500\times10^{-6}*25\times10^{-6}*8.8546\times10^{-12}}{2\left(2.25\times10^{-6}-\frac{2.25\times10^{-6}}{3}\right)^2}V^2-$$

$$\frac{2*6*500\times10^{-6}*25\times10^{-6}*8.8546\times10^{-12}}{2\left(20\times10^{-6}+\frac{2.25\times10^{-6}}{3}\right)^2}V^2-3.3295*\left(\frac{2.25\times10^{-6}}{3}\right)=0 \tag{3.14}$$

$$\Rightarrow 2.936\times10^{-7}V^2-2.49\times10^{-6}=0$$

This gives a pull-in voltage of

$$V_{pi}=\sqrt{\frac{2.49\times10^{-6}}{2.936\times10^{-7}}}=2.9163V \tag{3.15}$$

3.3.2 System Level Model

The Simulink model is created based on the system motion equations. The model can be found in Figure 3.3 where a voltage is applied to the microstructure and the mass of the system start moving. When the mass has reached the detector, in this case 2um, the simulation ends. Inside the model it can be seen that the forces are adding up together to determine the acceleration of the mass of the system as shown in Figure 3.4. From the figure it can also be seen that there is a damping model which calculate the damping force of the system. In this damping model, only the squeeze film damping is taken into account for calculating the damping force [18], since usually the squeeze film damping is much larger than the slide film damping. The squeeze film damping forces are usually generated by plates which are parallel orientated and moving parallel to each other. In this case the squeeze film damping due to the combs is the dominant one. The damping force is calculated based on the gap size which means that this system is a non-linear system.

Simulink Model Results

In this section two different simulations are presented. Both of them use an α of 1.009 where $\alpha*V_{pi}=V_{applied}$ is the applied voltage. The first situation is when the mass starts from the initial position and moves to the end of the gap. This graph is presented in Figure 3.5 and the nominal

pull-in time is 17.79ms. For the second situation the mass is moving from one end of the gap to the other end and in this case it is moving from the left end to the right end as presented in Figure 3.6 and the pull-in time takes up nominally 22.42ms. Figure 3.7 shows that the pull-in time is 4.032ms when the system moves from one end to the other end with an acceleration of -2g.

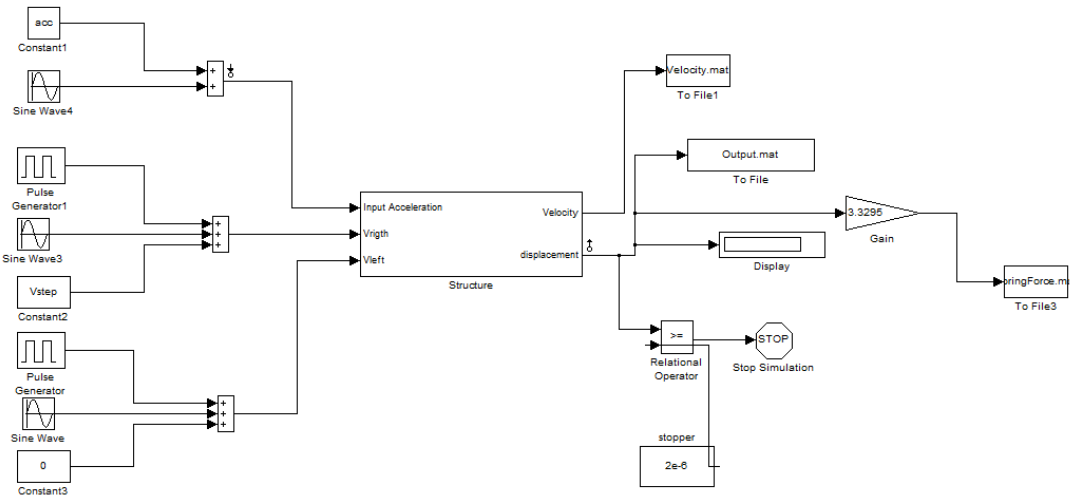

Figure 3.3 Simulink Model of the Pull-in Time Accelerometer

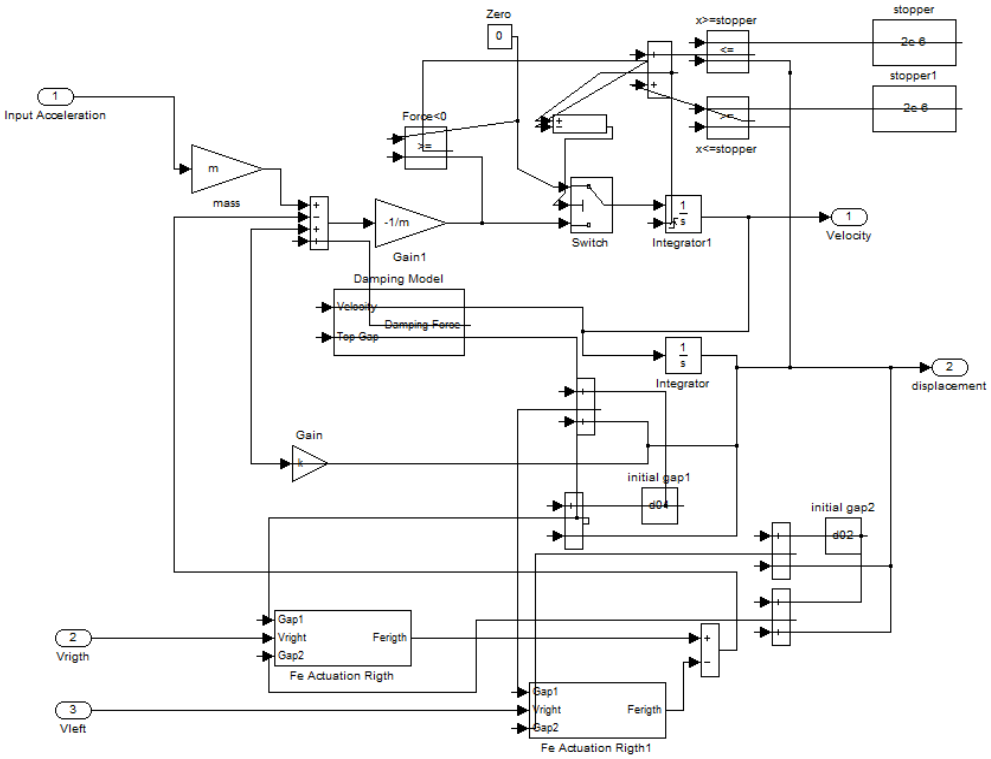

Figure 3.4 Simulink Model of the Pull-in Time Accelerometer 2

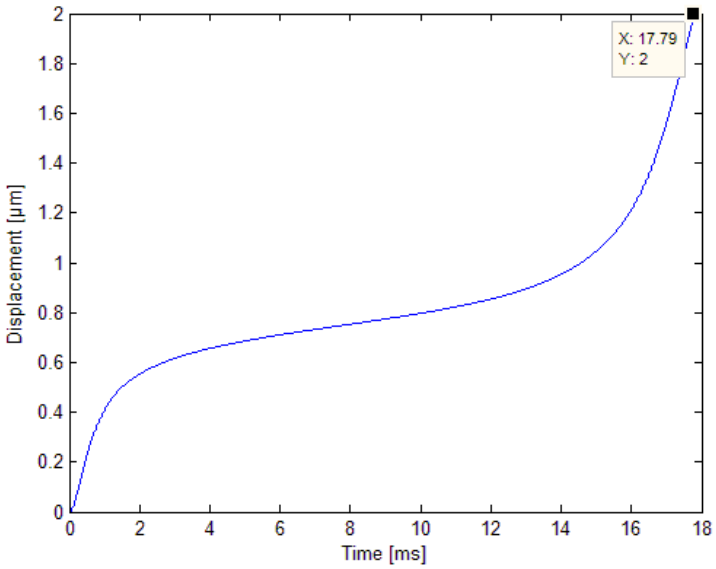

Figure 3.5 Pull-in Time Simulation Mass Moving From Rest State To 2 Microns

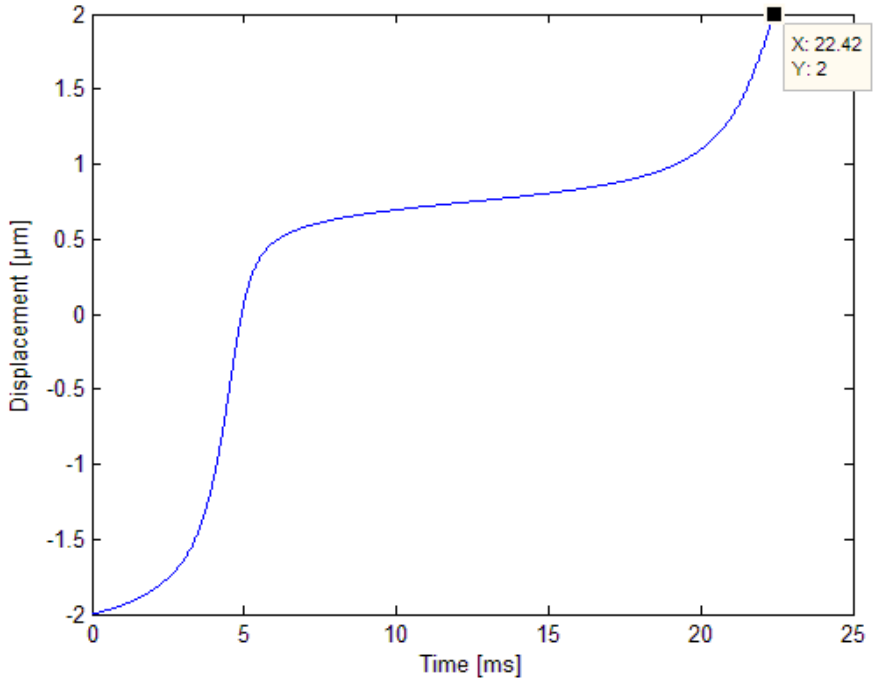

Figure 3.6 Pull-in Time Simulation Mass Moving From Left End (-2µm) To The Right End (2µm)

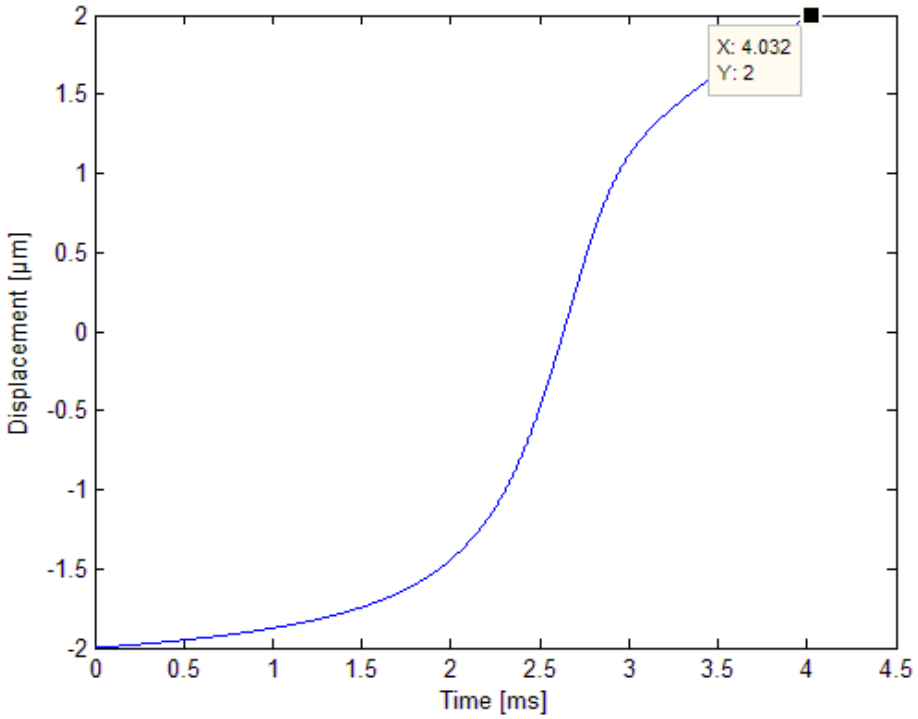

Figure 3.7 Pull-in Time Simulation Mass Moving From Left End (-2µm) To The Right End (2µm) With -2g Acceleration

3.3.3 Dynamic Range Issues

The pull-in time accelerometer system is driven by the electrostatic force that is generated by the electrodes. This means that if there is a force counteracting and is larger than the electrostatic force the accelerometer will fail to pull-in and the system does not work anymore as it should. In the static analysis of the system the only forces counteracting the electrostatic force are the spring force and the external acceleration force. The failure acceleration (maximum external acceleration leading to accelerometer malfunction), was estimated at different position within the range of interest. MATLAB was used to calculate these values and the results for a gap of 2.25µm at each side are shown in Figure 3.8. From Figure 3.8 the failure acceleration can be derived as around $0.2m/s^2$. The calculation was done based on the fact that the electric force generated by the combs needs to be larger than the mechanical force (forces due to the springs and external acceleration) plus the electric force generated due to anti-gap (Figure 3.9). The failure acceleration calculations were done using the next formula:

$$a_{failure} = \frac{F_{e,drivinggap} - (F_{m,spring} + F_{ext,acceleration} + F_{e,antigap})}{m} \quad (3.16)$$

Where $F_{e,drivinggap}$ is the electric force generated by the combs in the direction of interest (driving gap), $F_{m,spring}$ is the mechanical force generated by the springs, $F_{ext,acceleration}$ is the force generated by the external acceleration, $F_{e,antigap}$ is the electric force generated due to anti-gap and m is the mass of the proof mass.

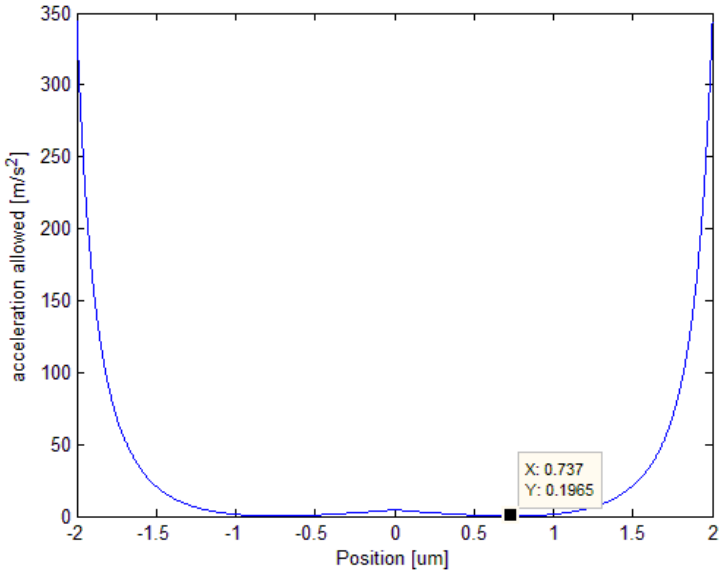

Figure 3.8 Failure Acceleration Between -2µm And 2µm With A Driving Gap Size Of 2.25um

Overcoming Failure Acceleration by Adjusting the Gap Size

One way to increase the failure acceleration is to adjust the gap size of interest. In this case the original driving gap size is 2.25um and the anti-gap size is 20um (Figure 3.9), leading to a total gap size of 22.5um. If the same total gap size is used but adjusting the gap size and the anti-gap size, a larger failure acceleration can be obtained as shown in Figure 3.10. Notice that the curve start decreasing if a certain value is reached. This is because the electrostatic force of the anti-gap is increasing and at that point it becomes significant to the system behaviour. The price that we need to pay for this increase is the increase of the applied voltage as shown in Figure 3.11. Moreover the system also becomes more underdamped, which means that the metastable region is getting smaller. From simulations it is found that with the current model with a total gap size (gap and anti-gap) of 22.5um the system starts to be underdamped at a gap size of around 4.5um (see Figure 3.12). So if the gap size is increased the damping should also be increased to remain in the overdamped region.

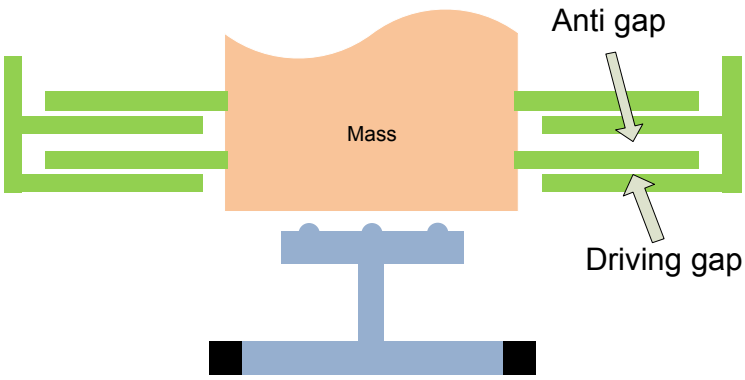

Figure 3.9 Accelerometer gap, anti gap definition

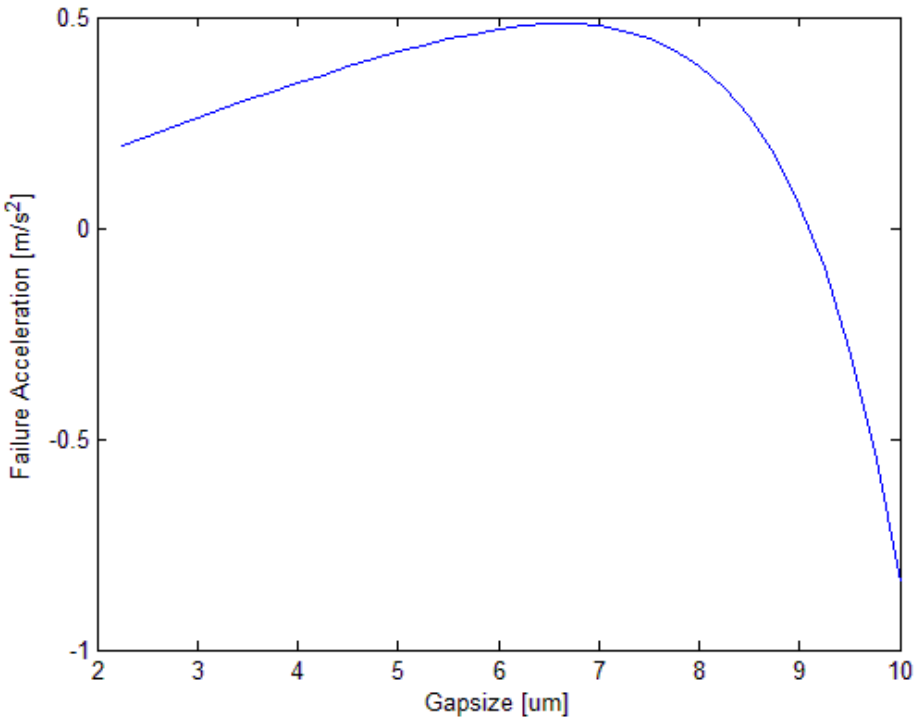

Figure 3.10 Failure Acceleration VS Gap Size

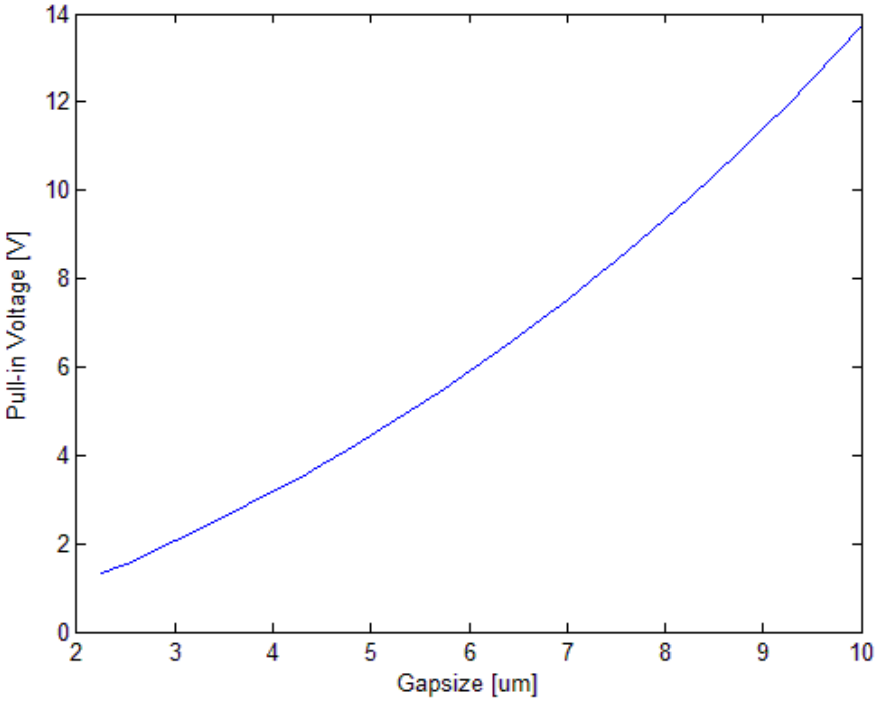

Figure 3.11 Pull-in Voltage VS Gap Size

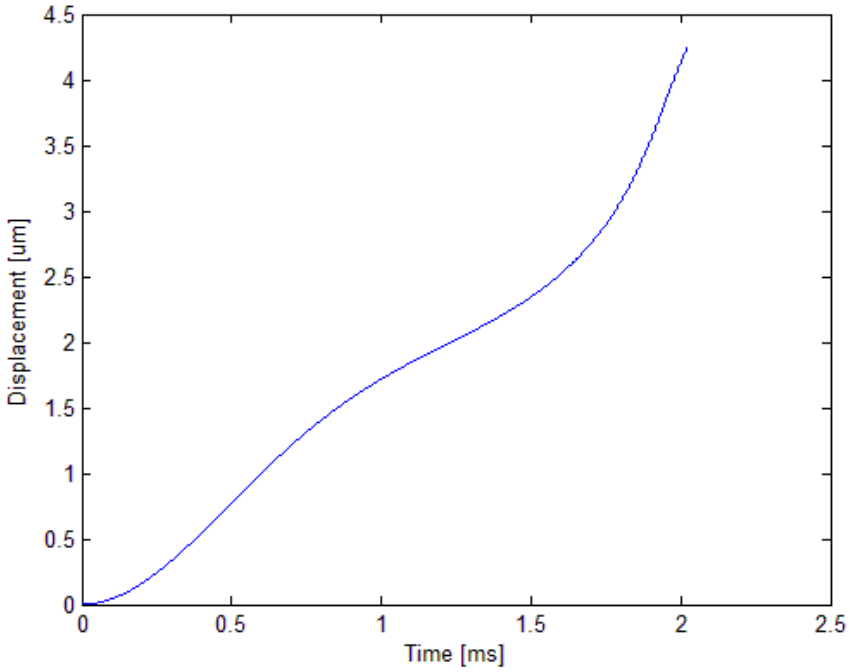

Figure 3.12 Pull-in Time With A Gap Size Of 4.5μm

3.4 Detector Design

Regarding the detector, the first thing that needs to be done is to design possible detector geometries and choose the best one. From the several envisaged designs the most promising geometries were chosen and compared with each other. These designs are shown in Figure 3.13.

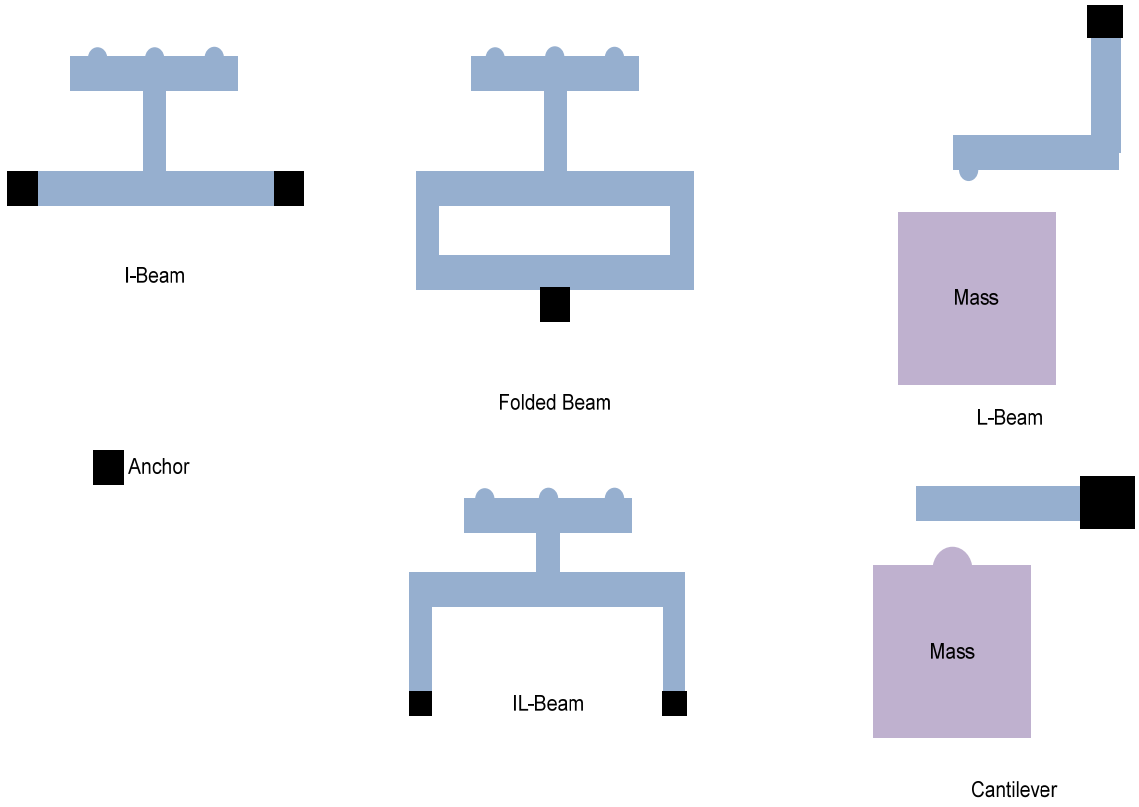

Figure 3.13 Top View Of The Possible Detector Designs

To determine which of the designs is the best one we need to know what the requirements are. In this case the detector should be able to detect if the mass hits it and on the same time the detector should not produce a signal due to noise vibration, so the detector has to be stiff not to be affected by the noise and it should not be too stiff to be able to measure the collision. The third requirement is that the detector should not bend too much but it should produce enough stress. These are the requirements for the detector. To compare the different structures with each other the third requirement has been considered. First, the curves for the force-stress and force-deflection relations were plotted and can be found in Figure 3.14 and Figure 3.15. These curves show that those relations are linear, meaning that the curve between the stress and the deflection is linear. Therefore, a stress-deflection ratio can be used to determine which structure should be used. These ratios can be found in Table 3.2. From Figure 3.14 it can be seen that the I-beam and the IL-beam have the highest stress-deflection, which means that the stress level for those two structures are higher than the other structures for the same deflection. These results reveal that the I-beam and the IL-beam are the best candidates for the detector. In Figure 3.16 the largest stress position is shown for the two structures and it can be seen that for the IL-beam case the largest stress is occurring far from the anchor. In case of designing a stopper both

structures are suitable to implement, but since the detector needs to be designed using piezoresistors, the closer the largest stress to anchor the better, due to wiring. Since wires on the detector will affect the output result of the piezoresistors. So the best candidate for this purpose is the I-beam. A COMSOL simulation picture of the I-beam is shown in Figure 3.17.

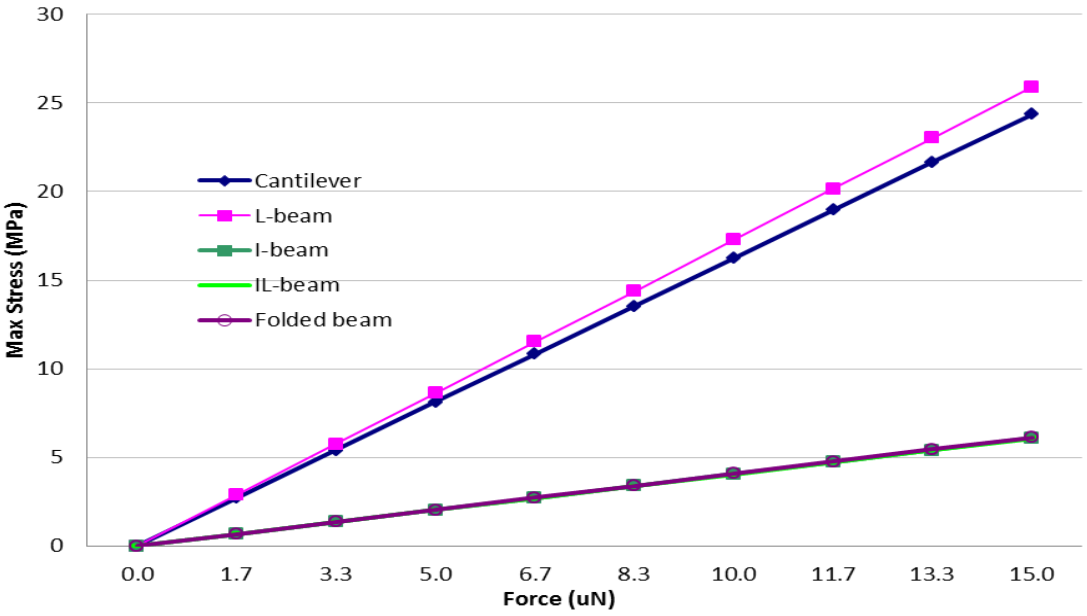

Figure 3.14 Force-Stress Curve Based On A Width Of 10μm

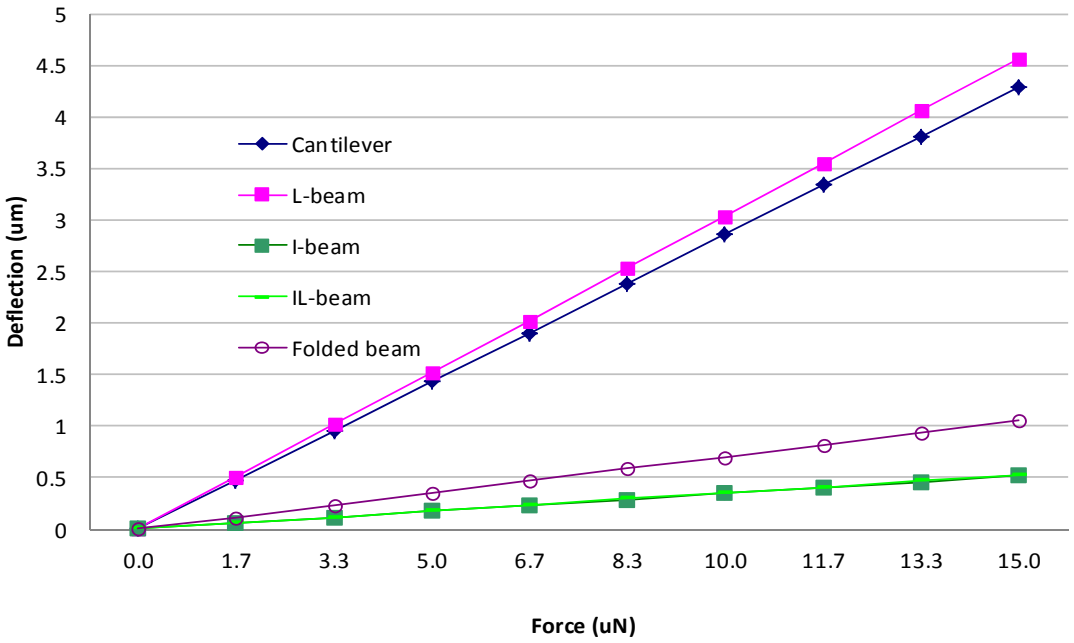

Figure 3.15 Force-Deflection Curve Based On A Width Of 10μm

Stress-Deflection Ratio	
I-beam	1.17e13 Pa/m
IL-beam	1.15e13 Pa/m
Folded beam	5.82e12 Pa/m
Cantilever	5.69e12 Pa/m
L-beam	5.68e12 Pa/m

Table 3.2 Stress-Deflection Ratio

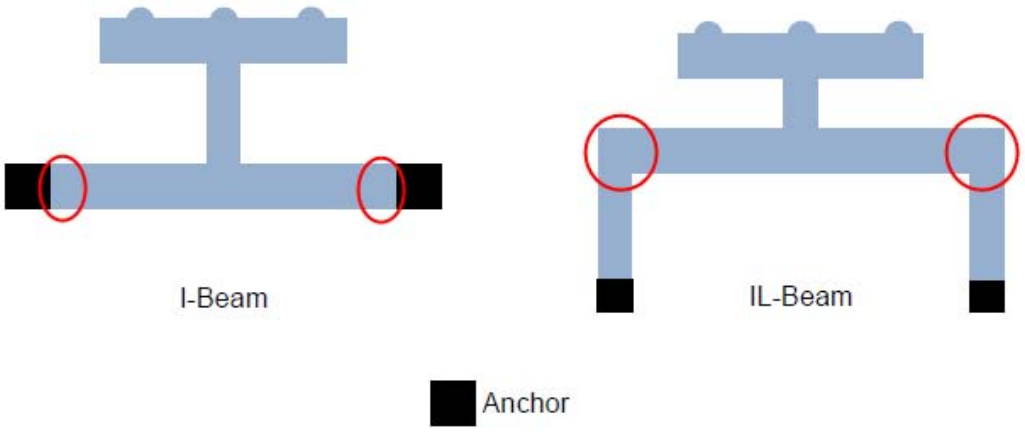

Figure 3.16 I-beam And IL-beam With Largest Stress Indication

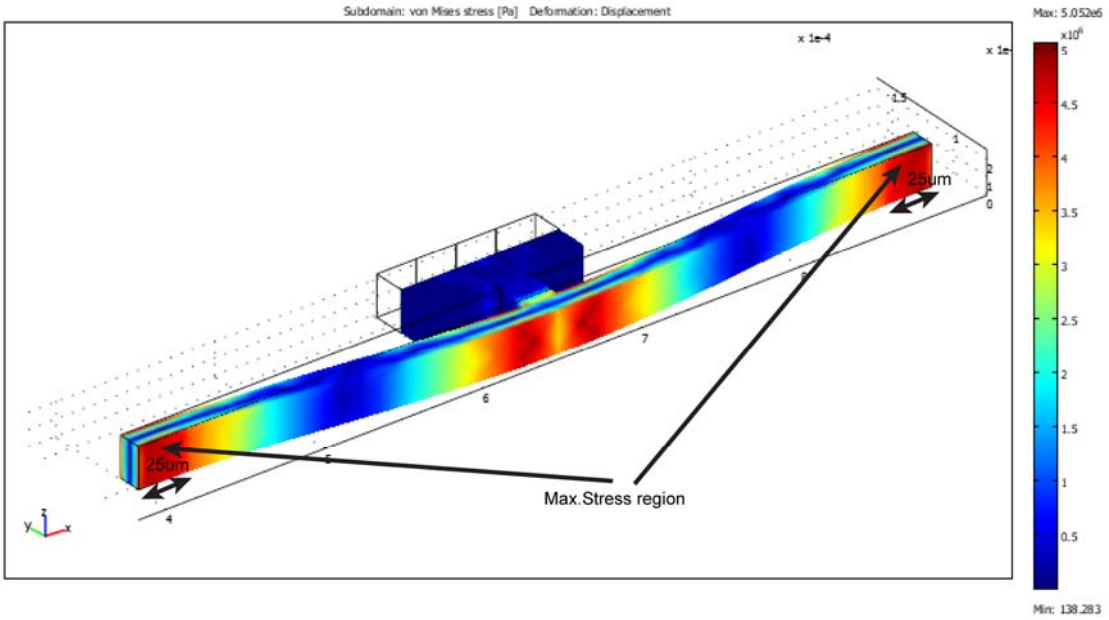

Figure 3.17 COMSOL Simulation I-beam

3.4.1 Piezoresistor Design

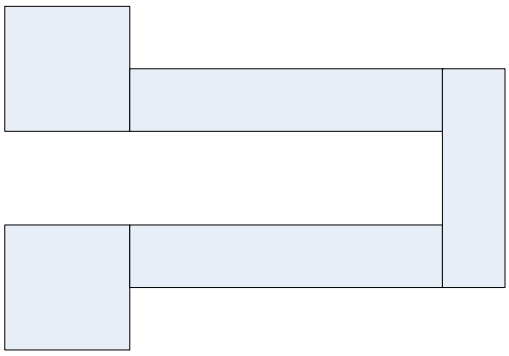

Figure 3.18 The Desired Shape Of The Piezoresistor For A Cantilever [29]

For a cantilever resistor a shape like the one given in Figure 3.18 is desired. Since in general the longitudinal gauge factor is larger than the transverse one a longitudinal piezoresistor is required. In order to neglect the ohmic contacts and the traverse part of the piezoresistor, those parts should be heavily doped. The longitudinal part of the piezoresistor needs to be moderately doped to provide a large gauge factor. The greater the doping is, the lower the gauge factor and resistivity. So the greater the doping the less influence the other parts of the resistor has on the gauge factor of the total piezoresistor. To reduce the influence of the other parts of the piezoresitor, a small resistance for these parts is desired. Using the resistivity calculator at the website of Brigham Young University [30] it can be seen that the resistivity of the p-type poly-silicon with a doping of $2\times10^{19}cm^{-3}$ is $0.0051\Omega cm$. So if the other parts have a resistivity that is much lower than this value the influences due to the other parts can be neglected.

Piezoresistor Dimension

Since only the detector needs to be sensitive in the lateral direction the Wheatstone bridge configuration suggested in [25] can be used with the u-shape piezoresistor shown in Figure 3.18. Figure 3.17 shows that the maximum stress will be at the two fixed ends. It also shows that the region of the max stress is from the fixed end to more or less $25\mu m$. So to let the piezoresistor remain sensitive the resistor should not be longer than $25\mu m$. It is assumed that at the neutral axis the bending stress will be zero and so the more the piezoresistor is placed at the border the sensitive the piezoresistor will be. Figure 3.17 also proves this. So the width has to be small to remain in the high stress region. Our design uses a width of $1\mu m$ and for the thickness the same value as suggested in [25], which is $0.5\mu m$ is used. The zero stress resistance for p-type silicon can then be calculated as (given in Eq.(2.13)) (doped with $1.1\times10^{18}cm^{-3}$ [25]):

$$R=\rho\frac{l}{A}=375\times10^{-6}\Omega m*\frac{25\times10^{-6}m}{1\times10^{-6}m*0.5\times10^{-6}m}=18.75k\Omega \qquad (3.17)$$

Electrical Noise in Wheatstone Bridge Circuit

The electronic circuit used for the read-out of piezoresistance is usually the Wheatstone bridge. Since the Wheatstone bridge contains resistors, it will generate noises where the thermal noise

and 1/f noise are the dominant ones [31, 32]. The equation of the equivalent noise voltage source for the thermal noise is given as [33]

$$\upsilon_n = \sqrt{4k_b TR\Delta f} \tag{3.18}$$

with k_b the Boltzmann constant ($1.3806503\times10^{-23} m^2 kgs^{-2}K^{-1}$), T the absolute temperature in Kelvin (300K usually), R the resistance and Δf the bandwidth. The accelerometer that we are using has a bandwidth of 44.6Hz (extracted from Figure 3.6). So the voltage noise, υ_n can be calculated as

$$\upsilon_n = 8.59\times10^{-10} * \sqrt{R} \tag{3.19}$$

It can be seen that the noise voltage is very small for a resistance of $18.75k\Omega\left(1.17\times10^{-7}V\right)$. The 1/f noise is given by the Hooge model as

$$V^2 = \frac{\alpha V_b^2}{N}\ln\left(\frac{f_{\max}}{f_{\min}}\right) \tag{3.20}$$

with α the dimensionless parameter, V_b the bias voltage across the resistor, N the number of carriers and f the frequency (assumed $f_{\min} = 10Hz$). Typical values for α are between 10^{-7} and 10^{-3} [32]. The resistor volume is $12.5\mu m^3$, and assuming V_b of 5V and a doping of $1\times10^{19} cm^{-3}$ gives a noise voltage of 17.29×10^{-6} volts. This means that the noise voltage cannot be neglected. Total noise is the sum of the noises in the four resistors [25].

$$4\left(\sqrt{\left(17.29\times10^{-6}\right)^2 + \left(1.17\times10^{-7}\right)^2}\right) = 69.6\mu V \tag{3.21}$$

To obtain a signal which is clearly above the noise level, the signal should be twice as large as the noise which means that the signal should be at least 139.2μV to cover all extreme cases. We assume that a p-type silicon is used with a gauge factor of 20 (value used in the rest of the dissertation to cover extreme cases). The design target is therefore, V_{out} = 139.2μV.

Read-out Circuit Configurations

When considering resistive readout circuits, the most commonly used circuit configurations are the voltage divider, half bridge and the full bridge. Next, the calculations for these configurations are done based on p-type silicon.

Voltage Divider

$$V_{out} = \frac{R}{2R + \Delta R}V_{in} \tag{3.22}$$

if a 5V input voltage is used.

$$139.2\times10^{-6}=\frac{R}{2R+\Delta R}*5\Rightarrow 27.84\times10^{-6}=\frac{R}{2R+\Delta R}\Rightarrow\frac{\Delta R}{R}=35917 \tag{3.23}$$

further it is given

$$GF*\varepsilon=\frac{\Delta R}{R} \tag{3.24}$$

$$20*\varepsilon=35917\Rightarrow\varepsilon=1795.85 \tag{3.25}$$

assuming a Young's modulus of $170GPa$, by Hook's law

$$\varepsilon=\frac{\sigma}{E} \tag{3.26}$$

$$1795.85=\frac{\sigma}{170\times10^{9}}\Rightarrow\sigma=3.05\times10^{8}MPa \tag{3.27}$$

Half Wheatstone Bridge

$$V_{out}=\left(\frac{R+\Delta R}{R+\Delta R+R}-\frac{R}{R+\Delta R+R}\right)V_{in}=\frac{\Delta R}{2R+\Delta R}Vin \tag{3.28}$$

$$139.2\times10^{-6}=\frac{\Delta R}{2R+\Delta R}*5\Rightarrow 27.84\times10^{-6}=\frac{\Delta R}{2R+\Delta R}\Rightarrow\frac{\Delta R}{R}=55.68\times10^{-6} \tag{3.29}$$

$$GF*\varepsilon=\frac{\Delta R}{R} \tag{3.30}$$

$$20*\varepsilon=55.68\times10^{-6}\Rightarrow\varepsilon=2.764\times10^{-6} \tag{3.31}$$

$$\varepsilon=\frac{\sigma}{E} \tag{3.32}$$

$$2.764\times10^{-6}=\frac{\sigma}{170\times10^{9}}\Rightarrow\sigma=0.473MPa \tag{3.33}$$

Full Wheatstone Bridge

$$V_{out}=\left(\frac{R+\Delta R}{R+\Delta R+R-\Delta R}-\frac{R-\Delta R}{R+\Delta R+R-\Delta R}\right)V_{in}=\frac{\Delta R}{R}V_{in} \tag{3.34}$$

$$139.2\times10^{-6}=\frac{\Delta R}{R}*5\Rightarrow 27.84\times10^{-6}=\frac{\Delta R}{R} \tag{3.35}$$

$$GF * \varepsilon = \frac{\Delta R}{R} \tag{3.36}$$

$$20 * \varepsilon = 27.84 \times 10^{-6} \Rightarrow \varepsilon = 1.392 \times 10^{-6} \tag{3.37}$$

$$\varepsilon = \frac{\sigma}{E} \tag{3.38}$$

$$1.392 \times 10^{-6} = \frac{\sigma}{170 \times 10^{9}} \Rightarrow \sigma = 0.236 MPa \tag{3.39}$$

3.4.2 Oscillations

After the mass leaves the detector, the detector will oscillate before it returns to its stable state. During the vibration there will be an interchange between kinetic and potential energy. When the mass hits the detector, the detector is bent and stressed, which means energy is stored in the detector. As the mass leaves the detector, it will restore to its stable state by releasing the energy. The energy is turned into kinetic energy which is represented by $\frac{1}{2}mv^2$. One important rule for energy is the conservation aspect. This means that all the potential energy will be changed to kinetic energy and vice versa. So the detector will oscillate and it would never stop if no energy loss is assumed. However, since the device is working in a viscous environment the detector will lose energy due to air damping. If the detector is modeled with a single DOF (degree of freedom) spring-mass-damper [34], the detector motion is described as

$$m\ddot{x} + c\dot{x} + kx = 0 \tag{3.40}$$

To solve this differential equation, assume that Eq.(3.40) has a general solution of the form

$$x(t) = ae^{\beta t} \tag{3.41}$$

and substituting this form into Eq.(3.40) yields

$$\left(m\beta^2 + c\beta + k\right)ae^{\beta t} = 0 \tag{3.42}$$

It can be seen that there is a trivial solution $x(t) = ae^{\beta t} = 0$, which corresponds to no motion. So this solution is not of interest. Eq.(3.42) can be rewritten in a characteristic form as

$$m\beta^2 + c\beta + k = 0 \tag{3.43}$$

The roots λ_1 and λ_2 are given by

$$\beta_{1,2} = -\frac{c}{2m} \pm \frac{1}{2m}\sqrt{c^2 - 4km} \tag{3.44}$$

The model can have three different motions, underdamped, critically damped and overdamped motion. The critical damping coefficient is given by

$$c_{cr} = 2\sqrt{km} \tag{3.45}$$

and the damping ratio is given as

$$\zeta = \frac{c}{c_{cr}} = \frac{c}{2m\omega} \tag{3.46}$$

where ω is the undamped natural frequency. Rewrite Eq.(3.44) yields

$$\beta_{1,2} = -\zeta\omega \pm \omega\sqrt{\zeta^2 - 1} \tag{3.47}$$

For the underdamped motion ($0 < \zeta < 1$) the solution is given as

$$x(t) = Ae^{-\zeta\omega t}\sin\left(\omega_d t + \phi\right) \tag{3.48}$$

where A is the initial magnitude, ω_d is the damped natural frequency ($\omega_d = \omega\sqrt{1-\zeta^2}$) and ϕ is the phase shift. For critically damped ($\zeta = 1$), the solution is given as

$$x(t) = e^{-\omega t}\left(a_1 + a_2 t\right) \tag{3.49}$$

where $a_1 = x_0$ and $a_2 = v_0 + \omega x_0$ (v_0 is the initial velocity, x_0 is the initial displacement of the mass). And for the overdamped case ($\zeta > 1$)

$$x(t) = e^{-\zeta\omega t}\left(a_1 e^{-\omega t\sqrt{\zeta-1}} + a_2 e^{\omega t\sqrt{\zeta-1}}\right) \tag{3.50}$$

where $a_1 = \dfrac{-v_0 + \left(-\zeta + \sqrt{\zeta^2-1}\right)\omega x_0}{2\omega\sqrt{\zeta^2-1}}$ and $a_2 = \dfrac{v_0 + \left(\zeta + \sqrt{\zeta^2-1}\right)\omega x_0}{2\omega\sqrt{\zeta^2-1}}$.

It can be seen in Eq.(3.48) that the e-power term is the one that returns the detector to its stable state ($x(t) = 0$). The $e^{-\zeta\omega t}$ term determines when the system is stable and this term will be zero only if $e^{-\infty}$. For this purpose it is found that $e^{-10} = 4.54\times10^{-5}$ and this is assumed to be approximately 0. Since the simulated pull-in time of the accelerometer in case of -2g acceleration is $\pm 4ms$ (moving both sides $\pm 8ms$), considering the stoppers at a $2\times10^{-6}\,m$ distance (Figure 3.7), it is reasonable to assume that the detector should return to its stable state in 1ms. If this requirement condition is assumed it becomes

$$\zeta\omega t \geq 10 \underset{t=1\times10^{-3}}{\Rightarrow} \zeta\omega \geq 1\times10^{4} \tag{3.51}$$

3.4.3 Impact

The impact is the largest force during operation and since the impact could damage the microstructure, it needs to be investigated. The impact force is given by

$$F = \frac{\Delta p}{\Delta t} = \frac{m\Delta v}{\Delta t} \tag{3.52}$$

The force depends on the time of contact. Since the time of contact between the mass and the detector is unknown, a worst case scenario situation should be considered. The worst scenario occurs when the mass hits the detector and stops immediately. In this case, the main concern with this force is that the structure should not be damaged. Impact analysis performed in [35], show that the impact time is around 1.5×10^{-7} seconds for a structure that is hitting a hard surface. In [36], experiments indicate that if a sensor accidentally falls from a height of 150cm the impact time on the package when it hits the ground is around 6×10^{-7} seconds so it can be concluded that the impact time should have a magnitude in the order of 10^{-7}.

3.4.4 Detector Design

It was already explained that the detector shouldn't be oscillating when the mass comes back to hit it again. In this situation, it was demonstrated that

$$\zeta\omega \geq 1\times10^{4} \tag{3.53}$$

which implies a large natural frequency

$$\omega = \sqrt{\frac{k}{m}} \tag{3.54}$$

However since stress is used as the measuring parameter the detector should not be too stiff, otherwise the desired output signal cannot be produced. So there is a design conflict that needs to be addressed. Since the first thing is to design a high resonance frequency structure the transduction resolution will be left for a second design stage. The detector is assumed to have squeeze-film damping which is modeled as two parallel plates. So the damping model that is used for the comb fingers is also used here. Since detector stability at 1ms is required, Figure 3.19 shows that at that time the mass is at $-1.876\mu m$. This suggests that the gap from the left detector is then $0.124\mu m$

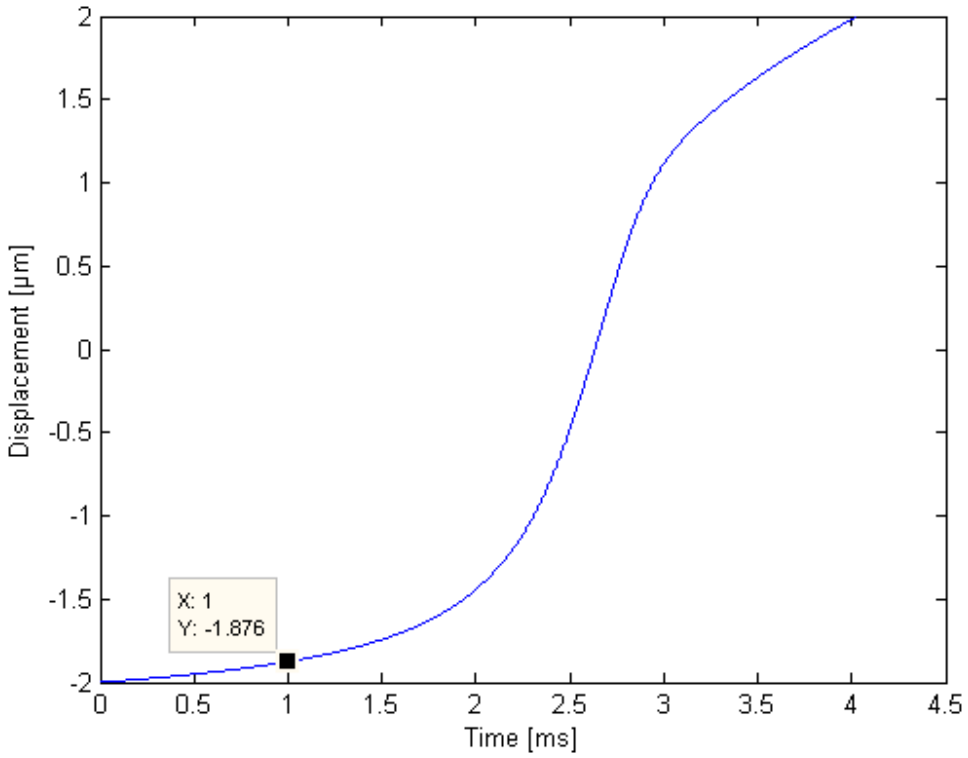

.

Figure 3.19 Pull-in Time Simulation Mass Moving To 2um From -2um With -2g Acceleration

Since we assumed that squeeze-film damping dominates over the other damping factors, the damping can be calculated. The calculation is done using the following method. Assume bumpers on the detectors of length $0.25\mu m$ are used and that the "contact bar" of the detector is $100\mu m \times 20\mu m \times 25\mu m (l \times b \times h)$. Because the mass is moving during oscillations the average damping is used, which is calculated by simulating the damping values for gap when $t = 0$ to $t = 1ms$. These values are added to each other and divided by the amount of elements used and this gives a damping coefficient of 1.66×10^{-4}. In order to fulfil the requirements of Eq.(3.53) the resonance frequency needs to be

$$\zeta\omega \geq 1\times10^{4} \Rightarrow \frac{1.66\times10^{-4}}{2\sqrt{km}}\sqrt{k/m} \geq 1\times10^{4} \tag{3.55}$$

at the same time the stress requirement needs to be considered. At $2\mu m$ the system has a pushing force of $85.49\times10^{-6}\,N$. The impact force is calculated as

$$F = \frac{\Delta p}{\Delta t} = \frac{m\Delta v}{\Delta t} = \frac{2.4851\times10^{-7} * 6.21\times10^{-4}}{1\times10^{-7}} = 1.5mN \tag{3.56}$$

The structure is required to generate a signal at collision and to survive the impact force due to collision. The design in Figure 3.17 was found by iterations. From the figure it can be seen that the stress is 5MPa, which is according to previous calculations enough to create a signal. To verify that the structure will sustain the impact force, a simulation was done and it shown a stress level of 91.07MPa. The yield stress of silicon is 1GPA so it can be conclude that the structure will survive the impact force. A yield force of 16.87N is found by iteration. The next calculations proved that vibration is not a problem. From the simulation the spring constant of the detector can be calculated as

$$k = \frac{F}{\delta} = \frac{85.49 \times 10^{-6}}{4.337 \times 10^{-8}} = 1.97 kN / m \tag{3.57}$$

The mass is calculated by

$$m = VolumeMass \times Density = 5.88 \times 10^{-10} kg \tag{3.58}$$

and Eq.(3.53) can be proven by filling in the parameters

$$\frac{1.66 \times 10^{-4}}{2\sqrt{1.97 \times 10^{3} * 5.88 \times 10^{-10}}} \sqrt{1.97 \times 10^{3} / 5.88 \times 10^{-10}} = 1.41 \times 10^{5} \geq 1 \times 10^{4} \tag{3.59}$$

The settling time is thus

$$\frac{10}{1.41 \times 10^{5}} = 0.07 ms \tag{3.60}$$

So it can be concluded that the design fulfils the needed requirements and it can be used in the system.

3.4.5 Different Possible Configurations

From earlier discussion it was decided to use the I-beam for the contact method. While using this contact method different possibilities for its implementation are shown in Figure 3.20 and Figure 3.21. In all these two designs collision between the mass and the detector occur. In the configuration shown in Figure 3.20, the mass will hit the detector as it moves towards that direction. After mass hits the detector they will move together by a displacement x (depends on the stiffness and the force that the mass has). When it reaches a certain point and a signal is detected by the read-out electronics the polarity of the electrodes will be turned and the mass will be pulled away from the detector. However because the detector is bend and it tries to recover its stable state, the detector will bend back and the mass will get an acceleration from the detector until the mass is out of reach for the detector. This might introduce errors, but if the acceleration that the mass will get is always the same then this error can be neglected. This method can be implemented as shown in Figure 3.22. The second system configuration (Figure 3.21) works different than the first two configurations. In this case the mass moves towards the detector and collides until a detectable signal is created. Then the mass will be pulled away (happening the

same thing as in the other two approaches) by the detector. When it moves away and reaches the other side, the same detector will be pulled by the mass to create the signal. This approach has the advantage of using only one detector, saving space on the chip. This approach can be implemented as shown in Figure 3.23.

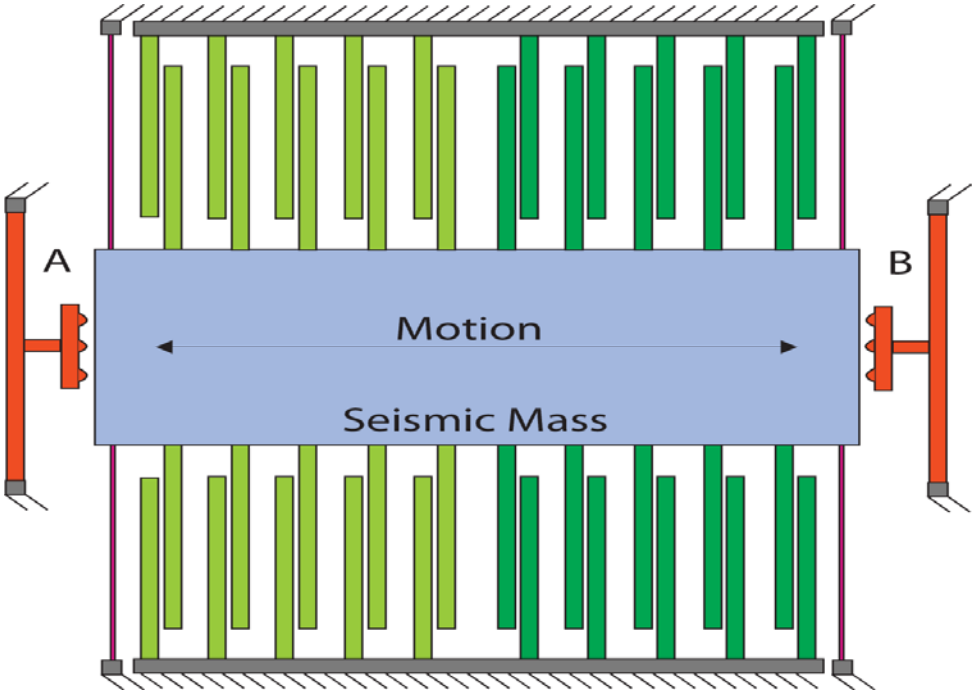

Figure 3.20 System Configuration 1

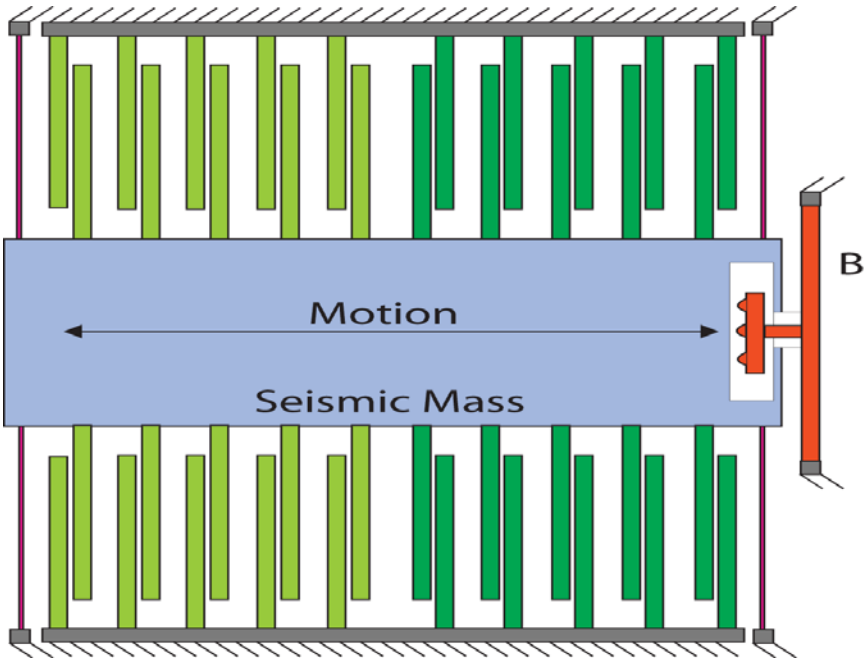

Figure 3.21 System Configuration 2

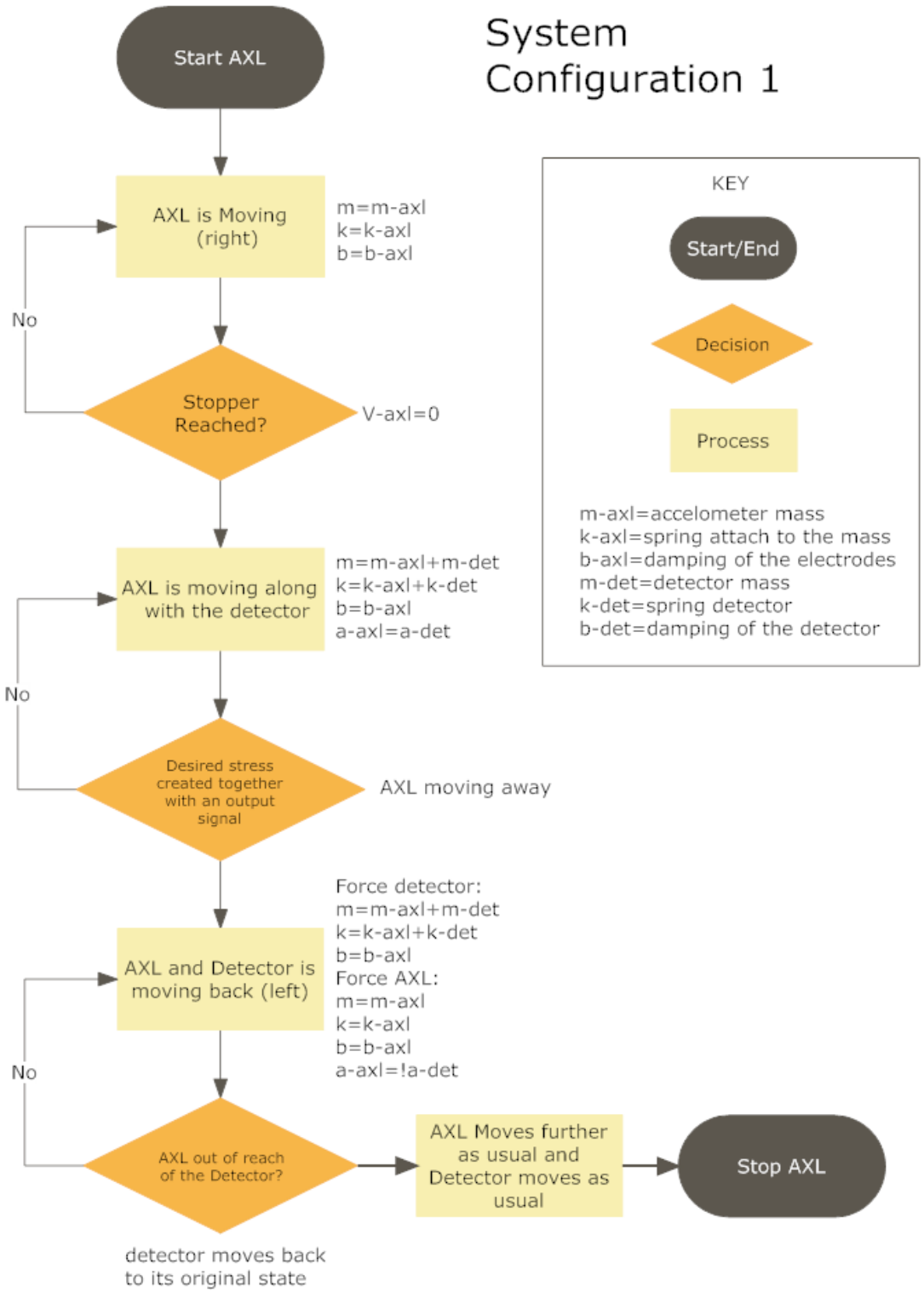

Figure 3.22 Work Flow Of System Configuration 1

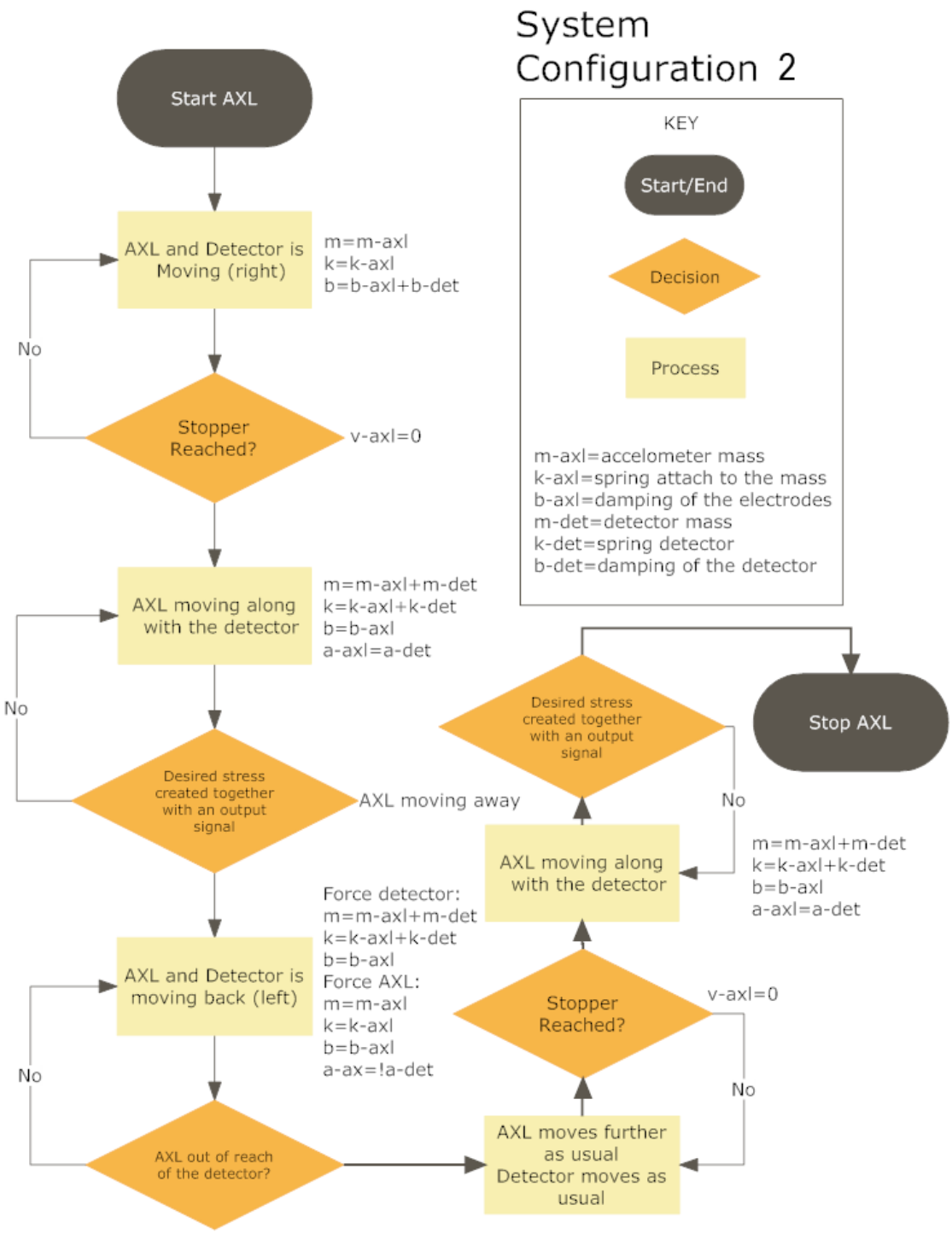

Figure 3.23 Work Flow Of System Configuration 2

3.4.6 Simulink Model of the Pull-in Time System with the Detector

The Simulink Model with the detector included can be found in Figure 3.24. In this figure the only difference with the previous model is that the mechanism to switch the applied voltage is added, so that when the pull-in event is detected, the mass is pulled to the opposite side. A few new blocks have been added to the system as shown in Figure 3.25. The detector is implemented in such a way, that when the mass reaches its destination it doesn't stop while pressing the detector, but rather the spring constant of the mass and the detector are added together in the simulation. When the mass is moving to the opposite direction the detector will push the mass back. An overview of this implementation is shown in Figure 3.22.

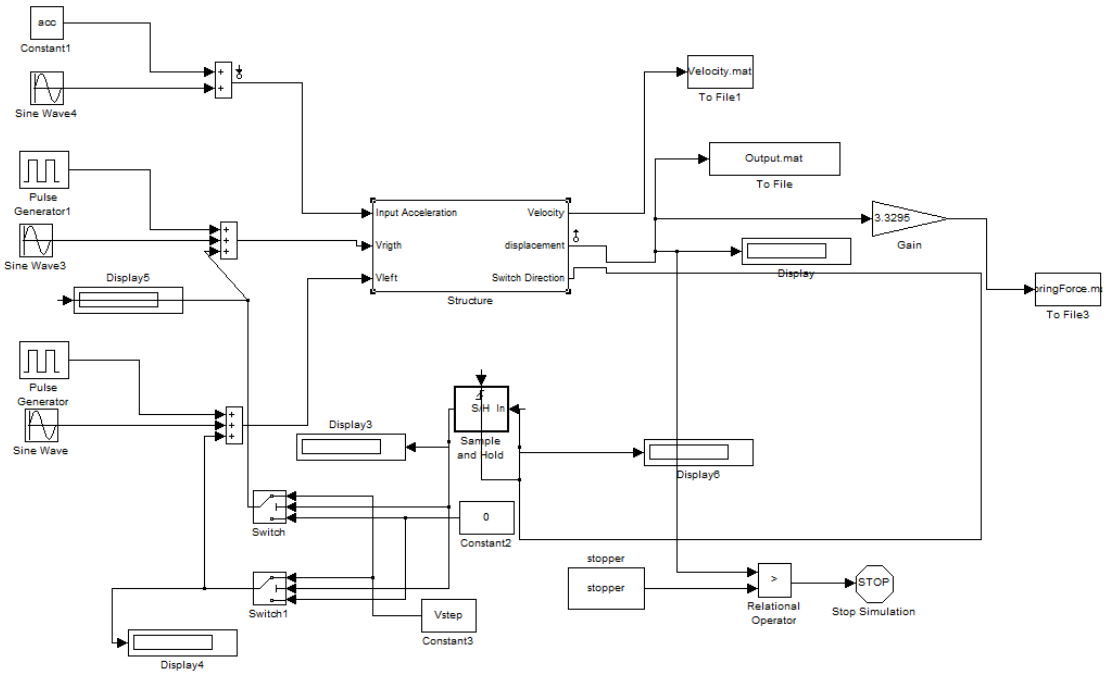

Figure 3.24 Simulink Model Of The Pull-in Time Accelerometer With Detector

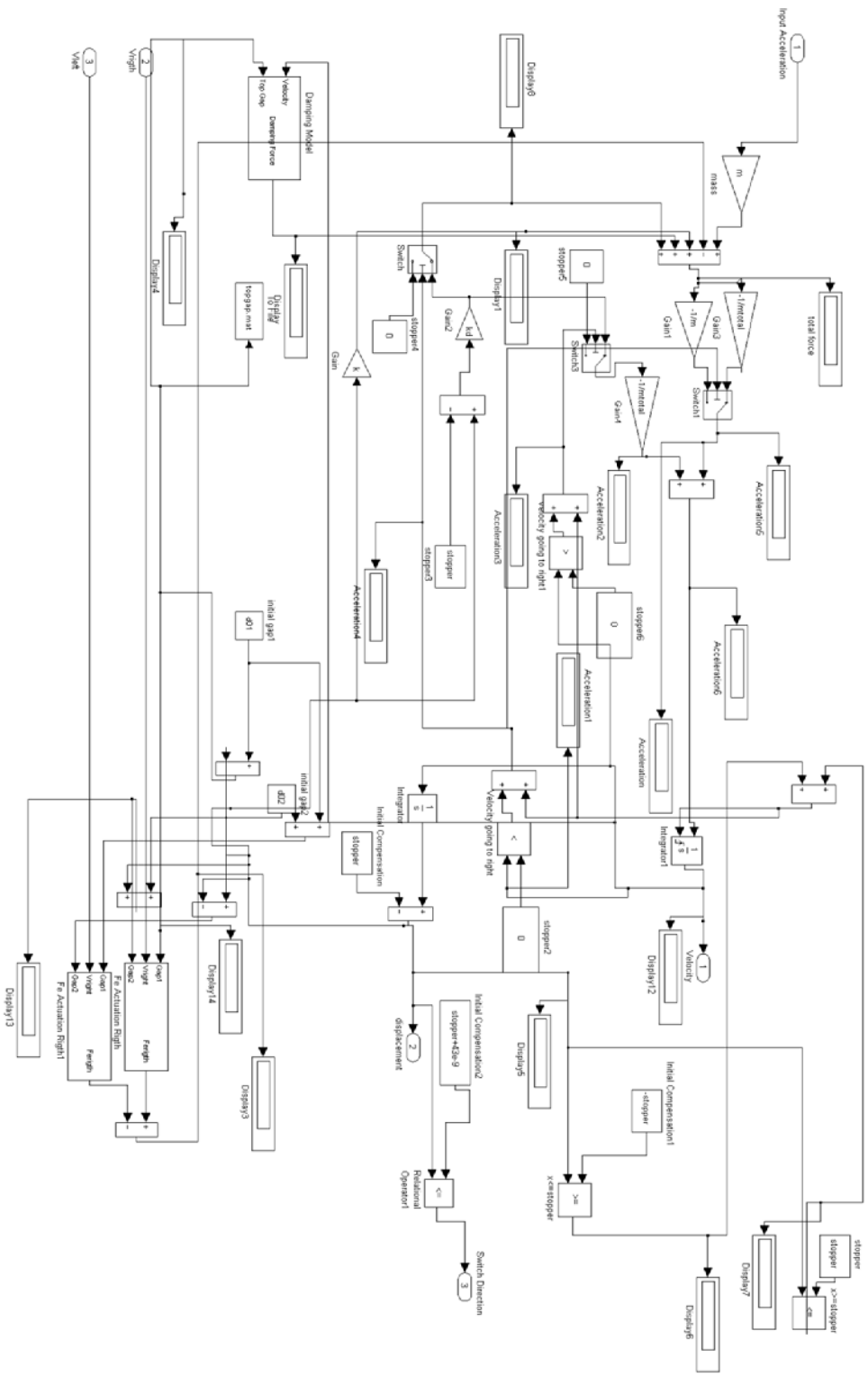

Figure 3.25 Simulink Model Of The Pull-in Time Accelerometer With Detector 2

Simulink Model Results

Initially, a simulation has been performed to check the detector when it returns to its rest state after being hit by the mass. The movement of the detector is shown in Figure 3.26. It can be seen that in the beginning the detector is hit and moves a certain distance, in this case 43nm.Then the detector returns to its rest state. While returning to its rest state, the detector pushes the mass back without oscillations. This happens due to the damping force of the accelerometer that absorbs the force of the detector (in this simulation it is assumed that there are no other forces acting on the mass since the force of the detector is dominating).

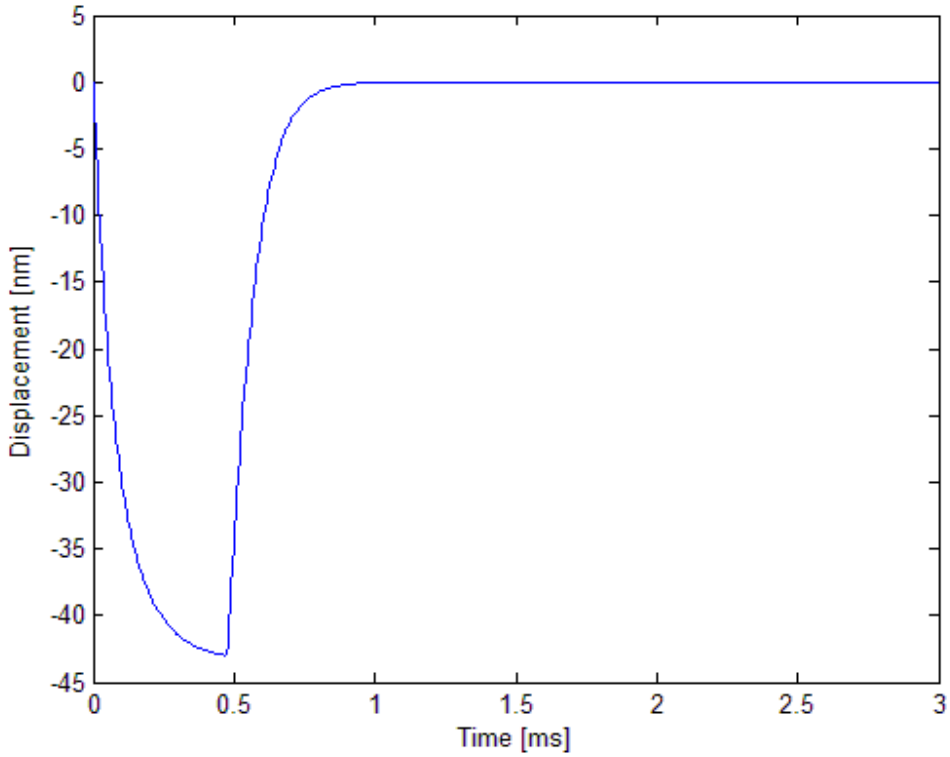

Figure 3.26 Detector Movement After It Got Hit By The Mass

Figure 3.27 shows the pull-time movement of the accelerometer, starting from the left side moving to the right side and after hitting the detector returning to the left side. Figure 3.27 also shows that detector use does not affect the behaviour of the accelerometer, which is a good indicator for real device operation.

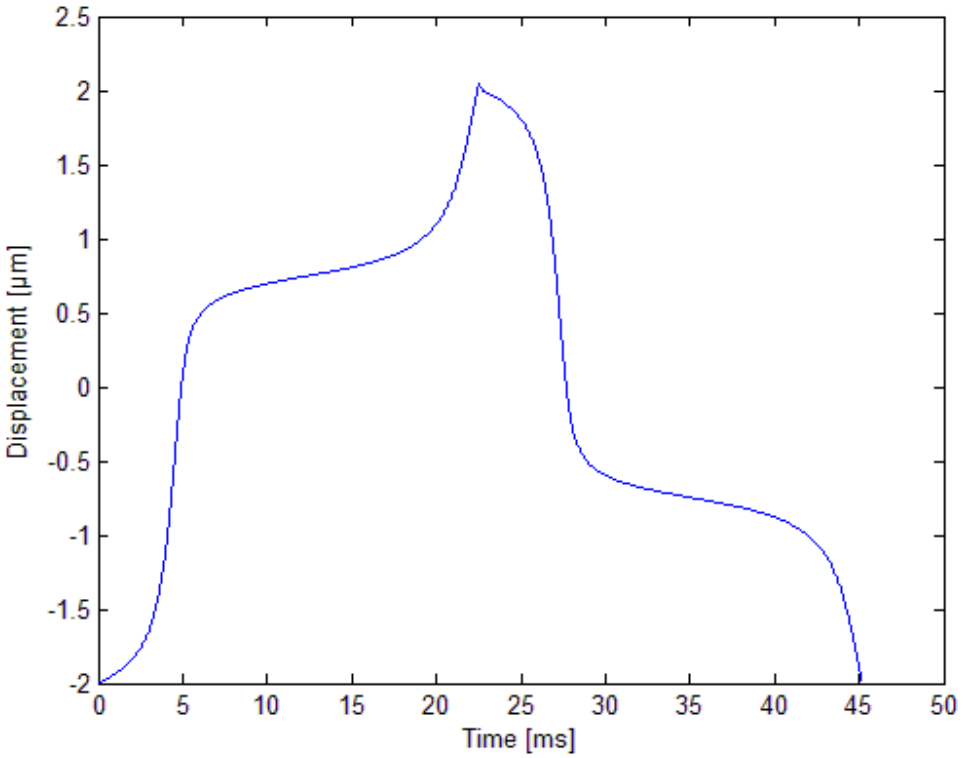

Figure 3.27 Simulation Result Of Configuration 1 and 2 (Moving To The Right Side And Returning To The Left Side)

3.5 Layout Designs

For the fabrication 2 layout designs have been made. The first one makes use of 2 flexible contacts. The second one is based on the same principle but with 1 detector only. These are shown in Figure 3.28 and Figure 3.29.

To make the designs with the desired parameters care needs to be taken due to the fabrication process and its limitations. One major concern is the under etching. Fabrication process under etch is common in DRIE processes, however how much the under etch will be is just an approximation. So designing a gap of 2um requires a gap of 1.12um since the under etch is expected to be approximately 440nm. From the design point of view the piezoresistors should be placed close to the edge of the detector where the generated stress is largest. So in the layout design the piezoresistors are placed 0.5 micron from the edge with the under etch of 0.44 micron considered. This is shown in the figure below. Extra bond pads are included in the designs to be able to ground the substrates.

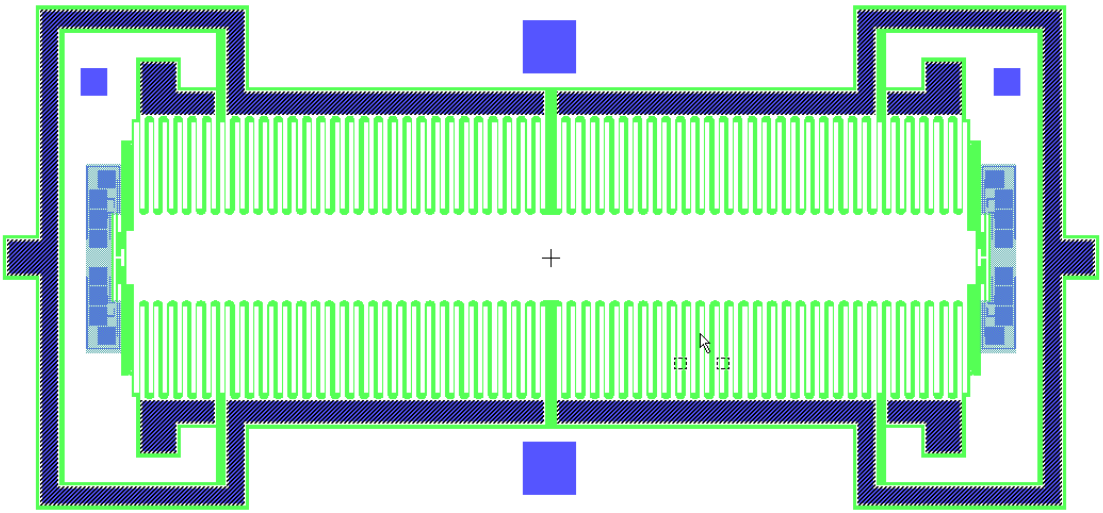

Figure 3.28 Layout System Configuration 1

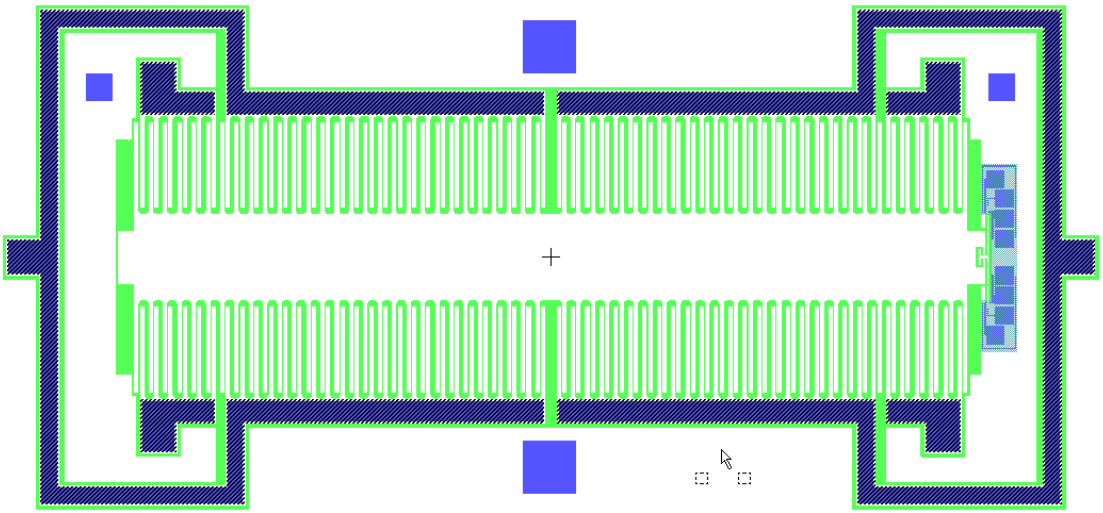

Figure 3.29 Layout System Configuration 2

4 Results

When it comes down to proposing new ideas and methods, the most interesting part are the experimental results. In this chapter the fabrication and measurement results of the piezoresistive detector are discussed based on [37]. The fabrication process is described step by step. Before the actual fabrication can start a layout file needs to be created according to the technology possibilities, which are limited by the fabrication facilities. A gap of 1um is considered to be feasible to fabricate. Moreover the fabrication process also includes uncertainties as undercuts. Other things that will be presented in this chapter are the measurement setups, configurations and results. The main focus of this dissertation is to show that piezoresistive detection can be used in time based pull-in accelerometers and therefore the mass should not get stuck with the detector and the detector should not break during the collision. Experimental results validate the piezoresisitve approach.

4.1 Fabrication Results

SOI-technology was used for the fabrication process of the devices. The final cross-section of the device is shown in Figure 4.1. The first step in the fabrication process was to grow a thin n-type epitaxial isolation layer on top of the SOI wafer. On top of the isolation layer a p-type epitaxial layer was grown that represents the piezoresistors. Because both the piezoresistors and the substrate were of the p-type material, an intermediate isolation layer was required. After the piezoresistors were etched a silicon nitride passivation layer was deposited onto the piezoresistors. This layer prevents the piezoresistors from oxidations. Later the silicon-nitride and the n-type isolation layer were etched, small contact holes were opened in the silicon-nitride layer to let the metal make contact with the piezoresistors. The next step was to deposit the metal on the wafer and at the unused places the metal was etched away. Oxide layer was added to the wafer to prepare the DRIE etching. The oxide layer will protect the other structures from the DRIE etching. When the structure was ready DRIE etching was applied. The last step of the fabrication process was to release the structure to make it movable.

Figure 4.3 shows clearly that the designed gap is not an issue at all for this fabrication process. Figure 4.2 shows the same results as the previous ones, no obvious fabrications errors are found. However Figure 4.4 shows that the metal lines that are connected to the piezoresistors are thinner than as drawn in the layout design. In the layout design the metal lines are drawn with 2 micron, however after it got fabricated the metal lines are approximately 1.4 micron and also not consistent everywhere. Although there is a difference in the width of the metal lines, it will not be a big issue as long as the metal lines are connected which is true in this case. From the same figure it is also shown that the piezoresistors are placed very much on the edge which is done on purpose as explained before.

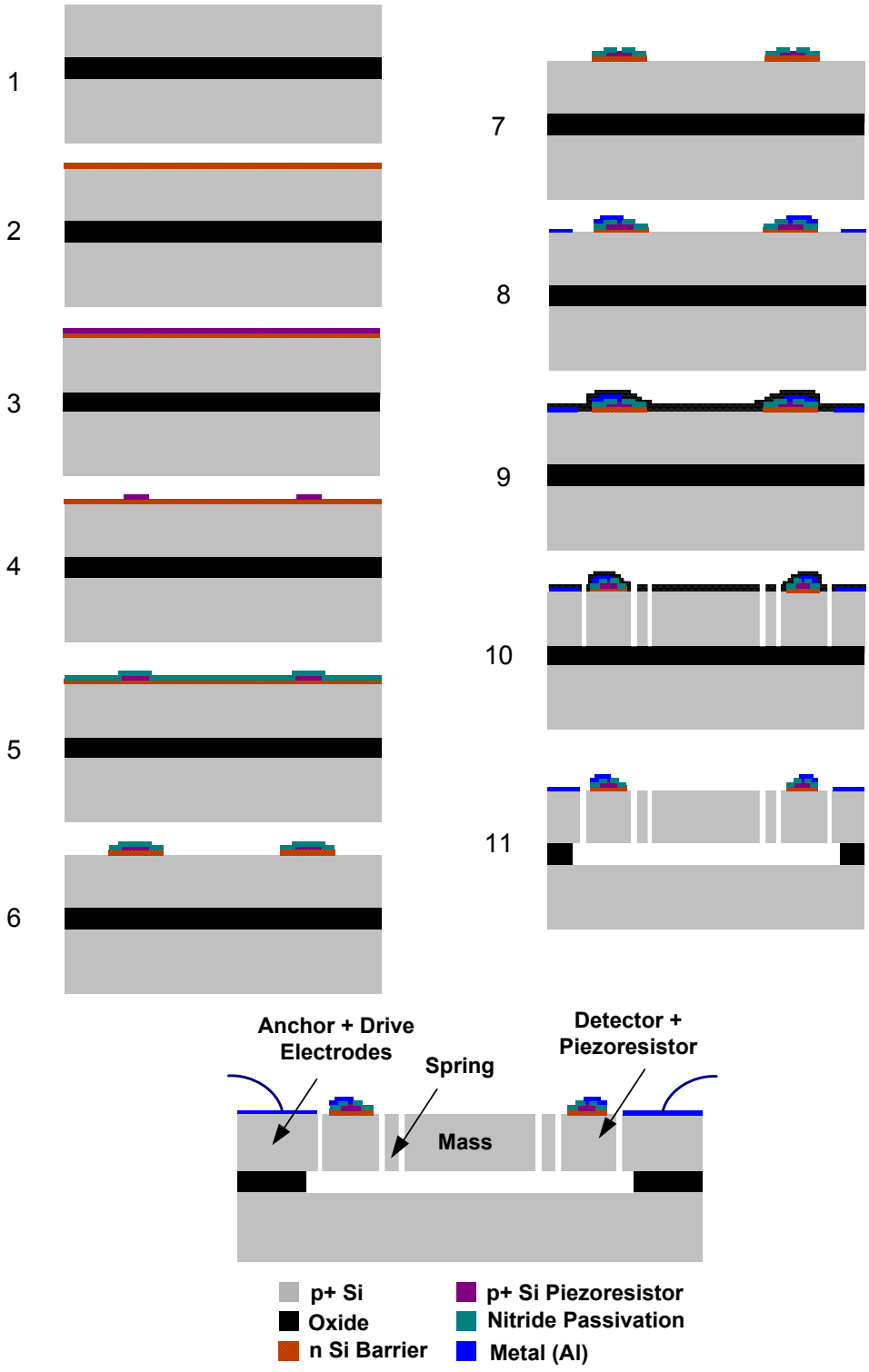

Figure 4.1 Fabrication process

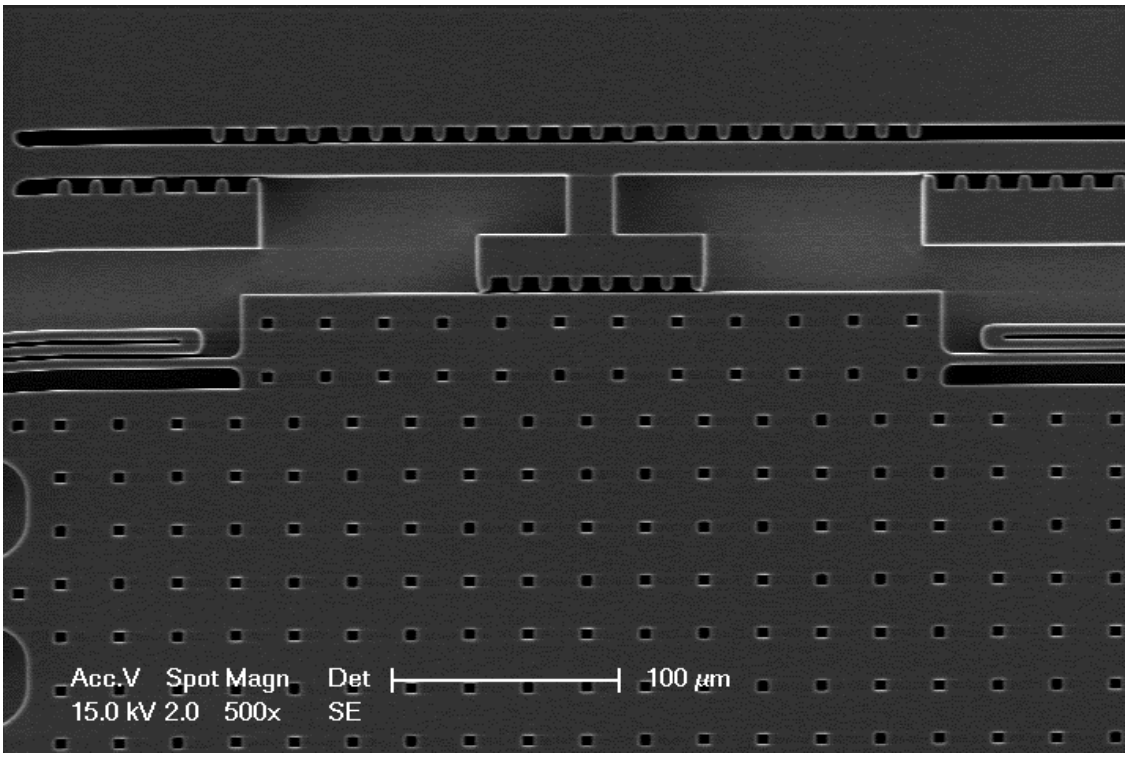

Figure 4.2 System Configuration 1

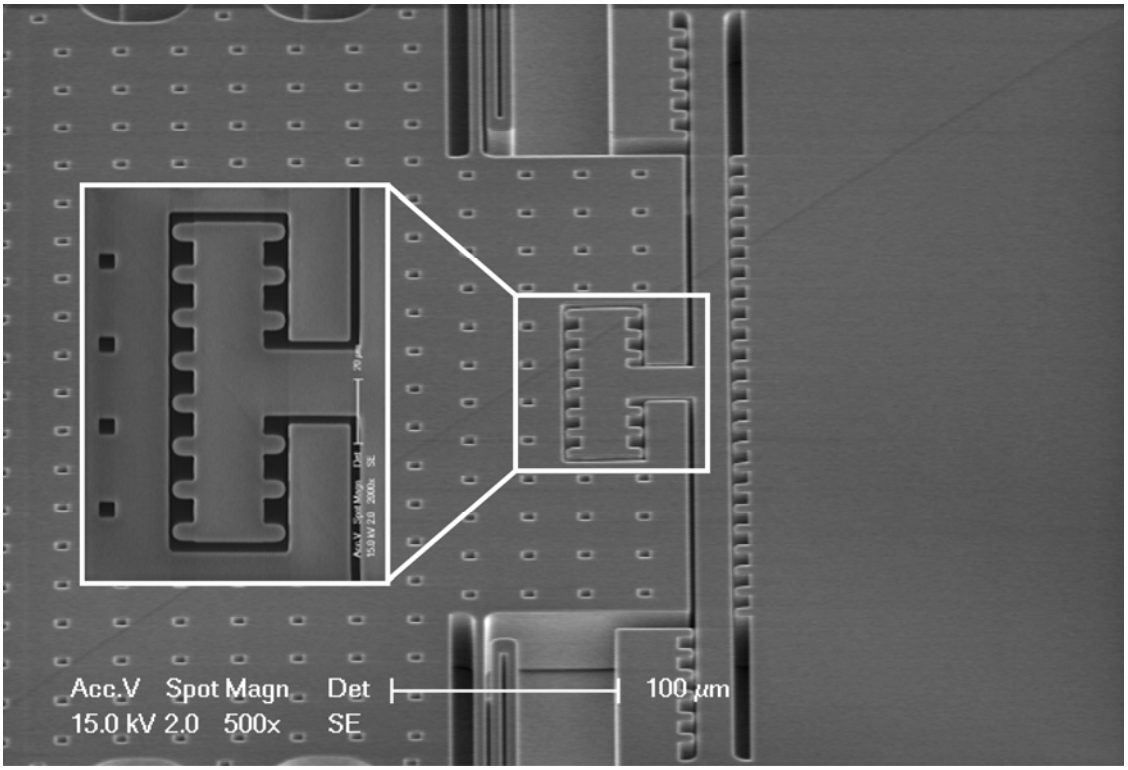

Figure 4.3 System Configuration 2

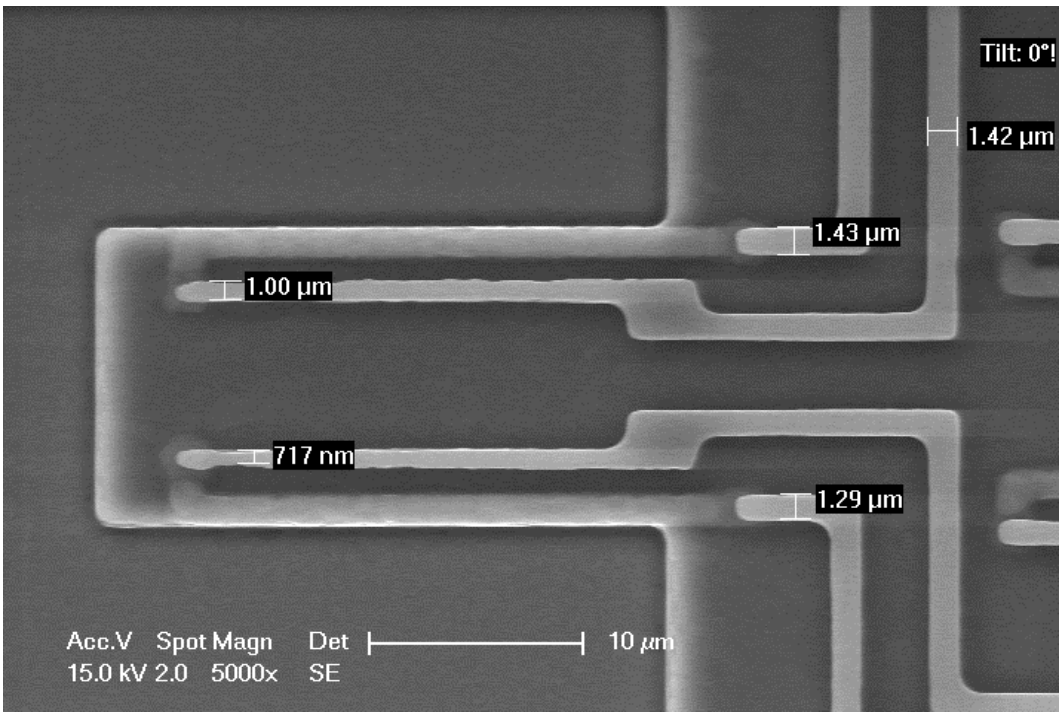

Figure 4.4 Piezoresistors With Metal Lines

4.2 Measurement Setup

To be able to do measurements on the chip, a measurement setup needs to be implemented. The measurements were done using the probe station HP4156, as shown in Figure 4.5. This probe station consists of six needles that can be used to drive or to measure the devices by placing the needles on the bondpads. The chuck (place where the chip is put) of the probe station can also be grounded to prevent any parasitic effects. The probe station is able to use the same needle to drive and sense at the same time. Using this probe station basic measurements can be done, which is enough to validate the detector principle.

4.3 Measurement Results

The goal of this project is to validate that the detector works as explained before. To get the signal out of the detector, piezoresistors are used. However before doing measurement on the Wheatstone bridge it would be very helpful if a separate piezoresistor is characterized. The piezoresistor is characterized using the configuration shown in Figure 4.6. As shown in the figure there are three bondpads: one is connected to the substrate and the other two are connected to the piezoresistor. By grounding the substrate the parasitic effects are minimized. Applying a potential over the piezoresistor, the piezoresistor can be characterized. The results are shown in Figure 4.7. It can be seen that the resistance is linear. The non-linearity is very small. Moreover the Wheatstone bridge is supposed to operate at 5V so we can consider that the resistance still behaves like a resistance and that the magnitude differences are not important for the targeted

application. From the graph it can be seen that the resistance is about $27.5k\Omega$, which is different from what was analyzed before. The differences are due to the dimension difference of the resistors. In fabrication ohmic parts were added to create contacts with the metal.

Figure 4.5 Measurement Setup

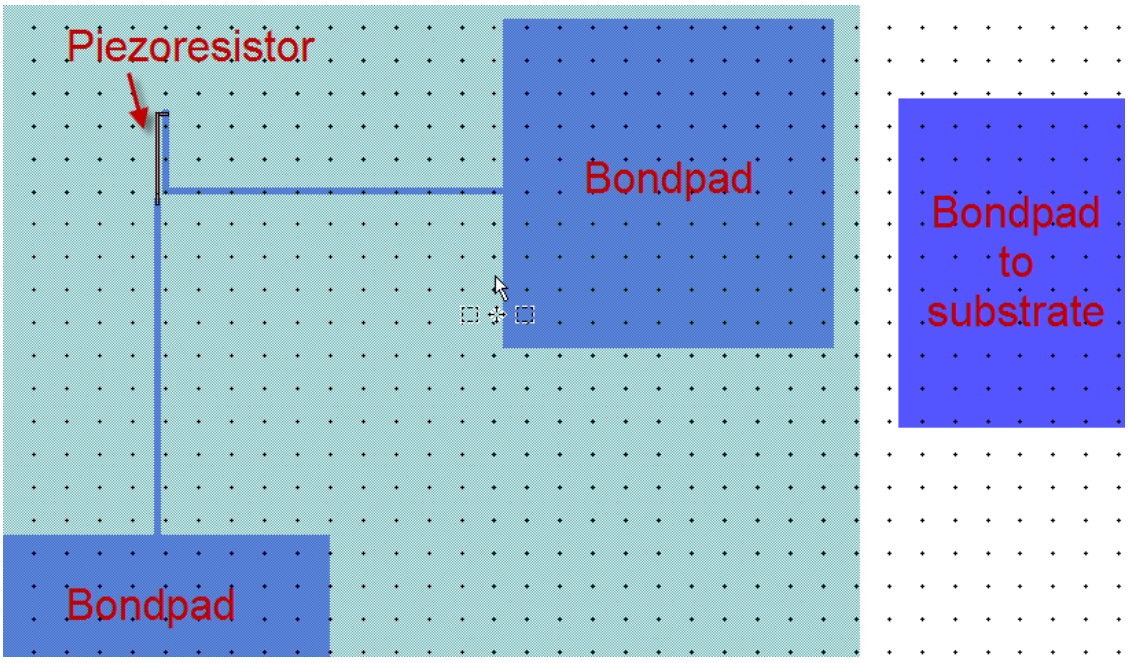

Figure 4.6 Piezoresistor Test Configuration

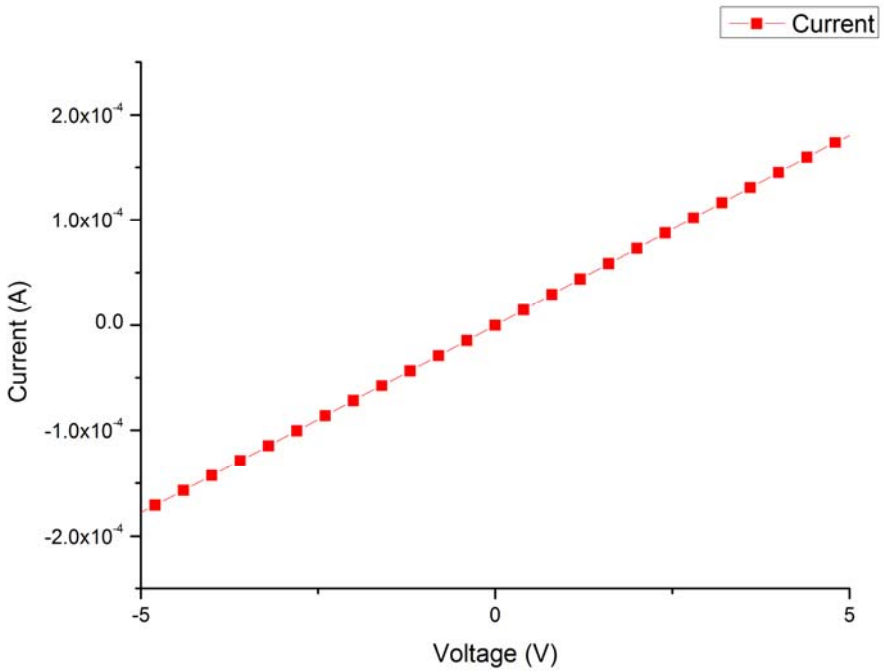

Figure 4.7 Piezoresistor Characterization

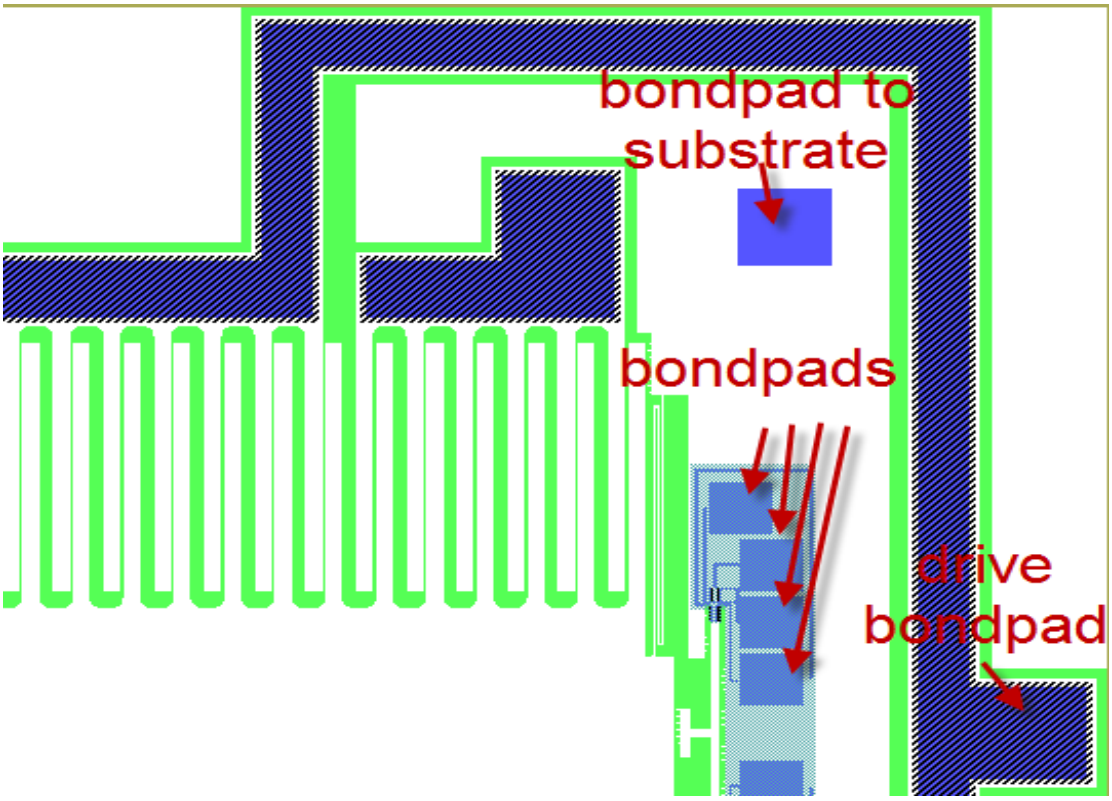

Figure 4.8 Measurement Configuration

To validate that the detector generates a signal when the mass collides, the configuration shown in Figure 4.8 is used. There is one bondpad to drive the mass and one bondpad to ground the substrate (mass) and four bondpads for read-out purposes. Note that the drive bondpad was originally designed for capacitive sensing. However due to measurement setup limitations it is used as the drive bondpad and 23 combs are driven instead of 6. The read-out can also be schematically shown in Figure 4.9. From measurement it is found that the resistances of the resistors are not the same. The measured values are listed in Table 4.1. Since the resistances are not the same, the bridge is unbalanced and will have an offset value at the output. In the Wheatstone bridge there are two piezoresistors that changes due to the stress, which are placed on the detector.

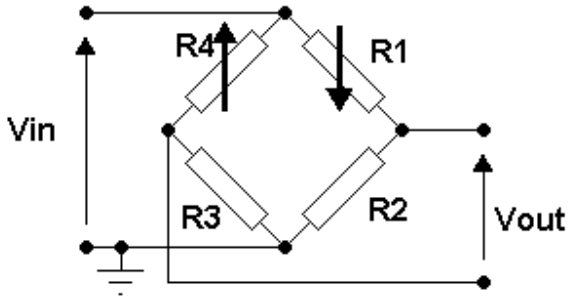

Figure 4.9 Measurement Read-out Schematic

Resistor name	Resistance (kΩ)
R1	23.67
R2	26.48
R3	26.19
R4	27.05

Table 4.1 Measure Bridge Resistances

Before the real device was tested, a test device was measured. The test device is shown in Figure 4.10. As shown in the figure behind the detector there are stopper to limit the detector movement. The stoppers were placed behind the detector with a distance of approximately 1um. The maximum displacement of the detector is limited by the electrode, which was approximately 5um from the detector. The measurement result is shown in Figure 4.11. The measurement was done mechanically, this means that the detector was mechanically pushed to the desired distance. It can be seen from the graph that the first part of the line is steeper than the last part. This is because the first part of the graph represented the detector movement up to 1um, which is before the detector hits the stopper. The last part of the graph described the detector from 1um till 5um. From 1um the detector moved further together with the stoppers, these limited the stress that was generated on the detector. The delta bridge output between 0um and 1um was 109mV, this is also the range of interest.

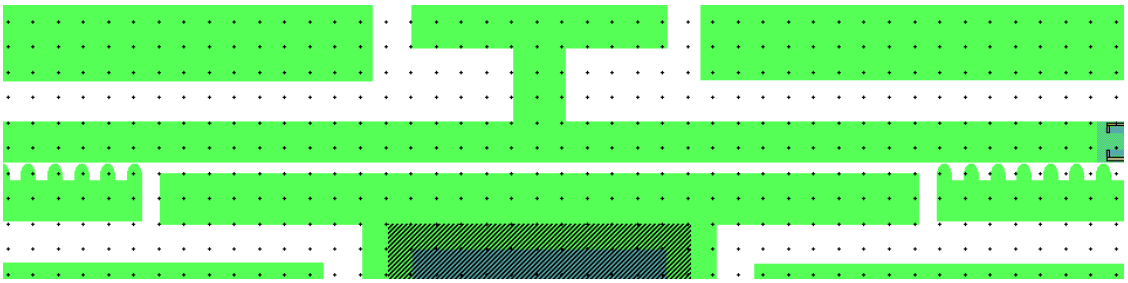

Figure 4.10 Test Device

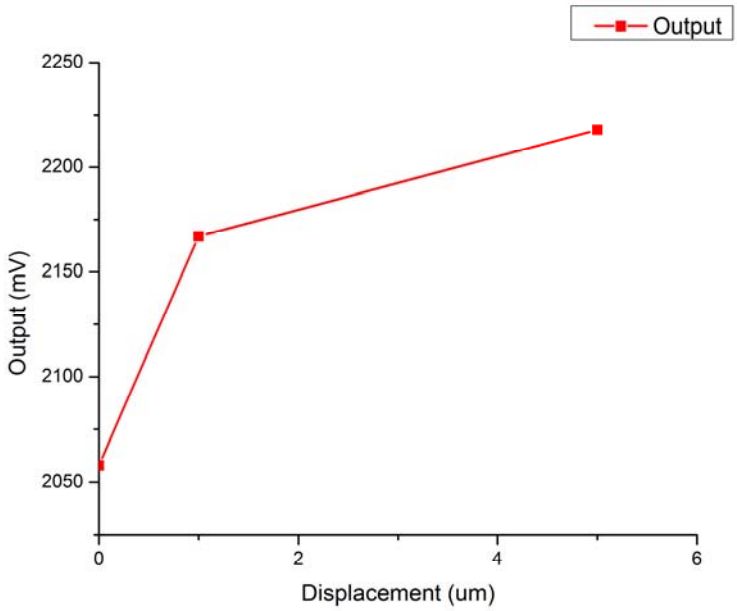

Figure 4.11 Test Device Measurement Results

The measurement results of the real device are shown in Figure 4.12. Figure 4.12 shows that there was 5mV difference between applied voltage of 6V and 10V (First pull-in point reached, Figure 4.13). This means that at this point the pull in has already occurred and there is enough stress generated to produce a signal. At 13V it can be seen that there was another delta output voltage of 35mV (in total 40mV). This means that there was a second pull-in. This was due to the collapsing of the electrodes (Second pull-in point reached, Figure 4.13). When the electrodes collapsed the detector was pushed with a total distance of approximately 400nm. This compromised with the measured results from the test device $\left(0.4 * 109_{1um,displacement} = 43.6mV\right)$.

An exact the same device but without detector has a pull-in voltage between 1.5 and 3 Volts [38]. From previous analysis the expected pull-in voltage was calculated as 2.92V for 6 drive combs, for 23 combs the pull-in voltage can be calculated as 2.11V. The measurements were done using 23 combs and therefore, voltages higher than 2.11V should pulled in the structure and generate a signal. The measured pull-in voltage found in [38] compromises with the calculated value. However the pull-in point of the detector can only be seen from 6 volts. This means that the force that is generated due to the electrodes was not enough for the detector to generate a detectable signal. The difference in pull-in voltages can be partly explained by the fact that there are lots of particles on the device as shown in Figure 4.14. So the pull-in voltage might differ from device to

device. The other part of the explanation was probably because the sensitivity of the detector was less than expected.

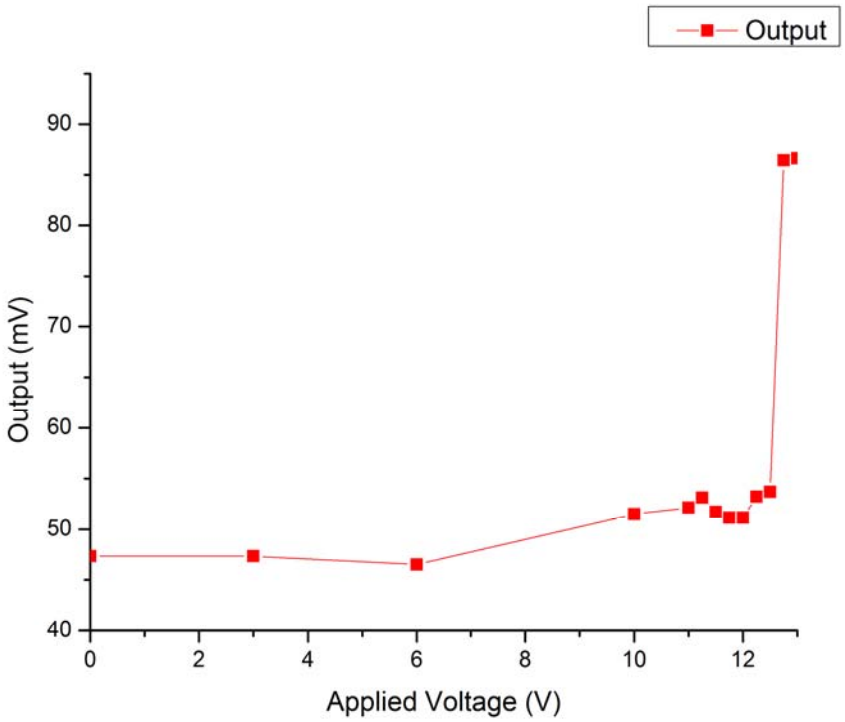

Figure 4.12 Measurement Results

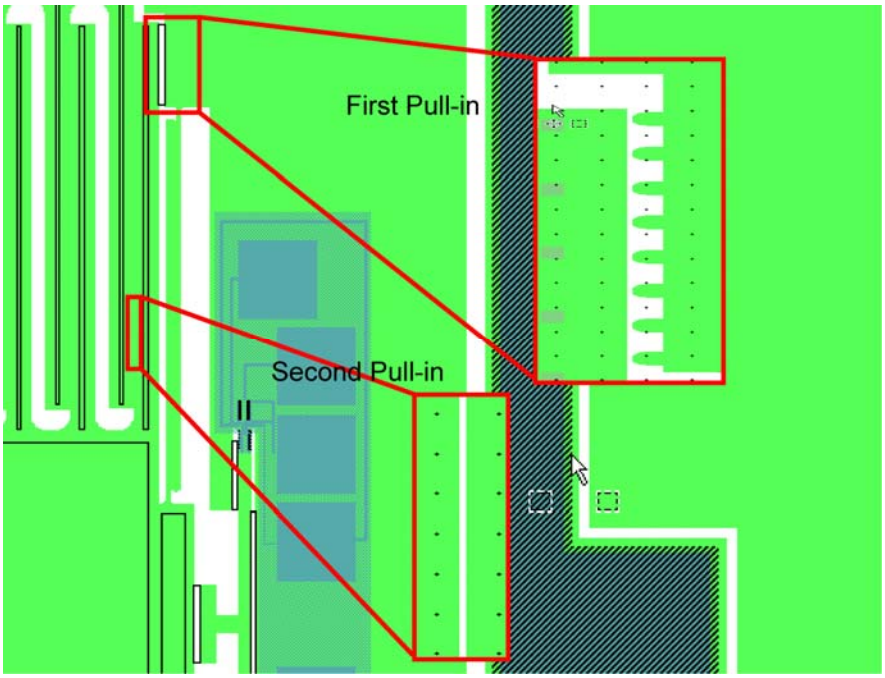

Figure 4.13 Accelerometer

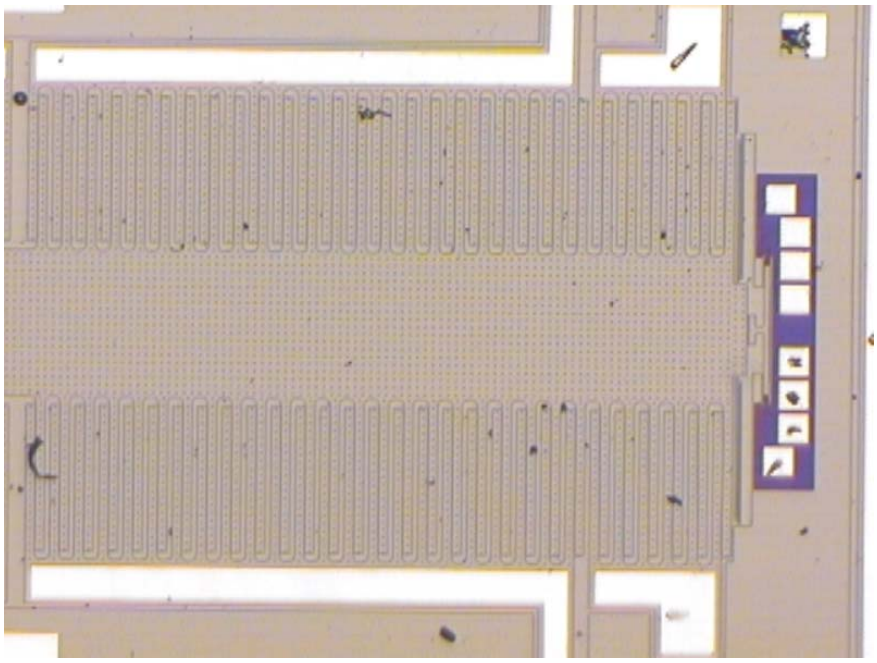

Figure 4.14 Fabricated Accelerometer

The sensitivity of the detector can be calculated as follows. When the detector was mechanically pushed by 400nm, the bridge output was approximately 40mV (Figure 4.11). So since the stress is linear proportional to displacement and stress is linear proportional to the bridge output, the sensitivity can be calculated as

$$Sensitivity = \frac{40mV}{400nm} = 0.1mV / nm$$

5 Conclusion

In this work the pull-in time accelerometer was introduced and analysed analytically as well as numerically. It was shown that the transition time is proportional to the acceleration. To measure the transition time, different transduction methods were proposed in literature. In this thesis the piezoresistive transduction method was introduced and also analysed. Different detectors were considered and the most suitable detector was chosen to implement. The detector was designed to generate the signal out of a collision and also to absorb a part of the collision force. This was meant to make the device more reliable (smaller impact force due to collision). The Wheatstone bridge configurations for the read-out purposes was analysed and implemented in the final devices. The piezoresistors which forms the Wheatstone bridge were designed according to the stress spectrum that was obtained from FEM simulations. For the contact method three stage behaviours were considered, before collision, at collision and after collision. The dynamic behaviour of the accelerometer and the detector were analysed and modelled using Simulink. The results of the Simulink simulations were shown in Chapter 3.

MEMS accelerometers were produced according to the layout file. The measurement results were obtained using the probe station HP4156. In Chapter 4, the measurement results were shown. The results show that the fabricated piezoresistors present different resistance values than the calculated ones. The main reason for this is because in the calculations only the piezoresistor was included, while the measured values also included the contacts points, so that increased the total volume of the piezoresistors. This resulted in a higher resistance value. The results also show that the detector generates a signal at around 6 volts which differs from the calculated one (2.11V). This is mainly due to lack of sensitivity of the detector and partly due to particles.

As a conclusion, the flexible contact method is a good alternative detection method and can be applied to MEMS based pull-in time accelerometers. This method can also be applied to other types of sensors, e.g. force sensors. However further investigations are required.

Future Work

The thesis has validated the piezoresistive detection method using flexible impact detectors. Since it was shown that using this method, signals were able to be generated due to pushing. However, the designed detector was too stiff to be sensitive enough to create a signal as the mass reaches the detector. Although it did generate a signal after the mass had pressed the detector with a certain force. So in the future the detector must be designed with a larger margin so that the sensitivity problem can be covered (detector should be less stiff). This can be done by decreasing the width of the detector. It might also be interesting to do a time test of the accelerometer along with the detectors and compare them with the previous works. Another interesting point is to do a test with the detector in combination with accelerometer capacitive readout. Using this combined detection method it would be possible to improve current knowledge on MEMS impact theory.

Publications

1. **B.S. Hau**, V. Rajaraman, L.A. Rocha, and P.J. French, “Pull-in time based acceleration sensing”, STW.ICT SAFE, Veldhoven, The Netherlands, November 2010.
2. V. Rajaramana, **B.S. Hau**, L.A. Rocha, P.J. French, and K.A.A. Makinwa, “Design and modeling of a flexible contact-mode piezoresistive detector for time-based acceleration sensing”, Proc. Eurosensors XXIV, Linz, Austria, September 2010, Vol.5, pp.1063-1066
3. V. Rajaraman, **Bou Sing Hau**, L.A. Rocha, R.A. Dias, R. Dekker, K.A.A. Makinwa, “A Novel SOI-MEMS “Micro-Swing” Time-Accelerometer Operating In Two Time-Based Transduction Modes For High Sensitivity And Extended Range”, Transducers 2011, Beijing, China, June 2011

References

[1] Cheng-Hsien Liu and Thomas W. Kenny, “A High-Precision, Wide-Bandwidth Micromachined Tunneling Accelerometer”, Journal of Microelectromechanical systems, September 2001, Vol.10 No 3, pp.425-433

[2] LM Roylance and JB Angell, “A batch-fabricated silicon accelerometer”, Electron Devices, IEEE Transactions on, December 1979, Vol.26, pp. 1911-1917

[3] Multimems, 2007, *http://www.multimems.com/Offer/Exp_Acceleration.htm*, access date: February 2011

[4] L.Mol, L.A.Rocha, E.Cretu, and R.F.Wolffenbuttel, “Pull-in time based high sensitivity accelerometer with adjustable range and resolution”, Technical Digest, MME06, 2006 pp.129-132

[5] D.L. DeVoe and A.P. Pisano, “A fully surface-micromachined piezoelectric accelerometer”, Transducers 1997, Chicago, USA, June 1997, Vol.2, pp.1205-1208

[6] V. Rajaramana, B.S. Hau, L.A. Rocha, P.J. French, and K.A.A. Makinwa, “Design and modeling of a flexible contact-mode piezoresistive detector for time-based acceleration sensing”, Proc. Eurosensors XXIV, Linz, Austria, September 2010, Vol.5, pp.1063-1066

[7] B.S. Hau, V. Rajaraman, L.A. Rocha, and P.J. French, “Pull-in time based acceleration sensing”, STW.ICT SAFE, Veldhoven, The Netherlands, November 2010.

[8] Terry V. Roszhart, Hal Jerman, Joe Drake, and Constant de Cotiis, “An inertial-grade, micromachined vibrating beam accelerometer”, The 8th International Conference on Solid-State Sensors and Actuators, and Eurosensors IX, Stockholm, Sweden, June 1995, pp.656-658

[9] T. Korhonen, “Three-dimensional hall effect accelerometer for recording head movements of freely moving laboratory animals”, Physiology & Behavior, USA, March 1991, Vol.49 No.3, pp.651-652

[10] KL Phan, A. Mauritz, and FGA Homburg, “A novel elastomer-based magnetoresistive accelerometer”, Sensors and Actuators A: Physical, 2008, Vol.145, pp.109-115

[11] AM Leung, J. Jones, E. Czyzewska, J. Chen, and B.Woods, “Micromachined accelerometer based on convection heat transfer”, MEMS 98, Heidelberg, Germany, January 1998, pp.627-630

[12] U.A. Dauderstädt, “A Thermal Accelerometer”, PhD thesis, TU Delft, Delft, The Netherlands, 1999, ISBN 90-407-1885-7 / CIP

[13] C. Yeh and K. Najafi, “A low-voltage bulk-silicon tunneling-based microaccelerometer”, International Electron Devices Meeting 1995, Washington DC, USA, December 1995, pp.593-596

[14] C.H. Liu, A.M. Barzilai, J.K. Reynolds, A. Partridge, T.W. Kenny, J.D. Grade, and H.K. Rockstad, “Characterization of a high-sensitivity micro-machined tunneling accelerometer with micro-g resolution”, Journal of Microelectromechanical Systems, June 1998, Vol.7 No.2, pp.235-244

[15] NC Loh, MA Schmidt, and SR Manalis, “Sub-10 cm^3 interferometric accelerometer with nano-g resolution”, Journal of Microelectromechanical Systems, June 2002, Vol.11 No.3, pp.182-187

[16] H. Yang, L. Pakula, and PJ French, “A novel operation mode for accelerometers”, Pacific Rim workshop on transducers and micro/nano technologies, Xiamen, China, July 2002, pp.303-306

[17] H. Yang et al, “Design of a vertical surrounding gate jfet for capacitive sensing based on soi-mems technology”, internal report. Internal Report, State Key Laboratory of Transducer Technology, SIMIT, Shanghai, PR China (unpublished)

[18] L.A. Rocha, “Dynamics and Nonlinearities of the Electro-Mechanical Coupling in Inertial MEMS”, PhD Thesis, TU Delft, Delft, The Netherlands, 2005, ISBN 90-8559-025-6

[19] J.M. Gere and P. Timoshenko, “Mechanics of Materials”, Third SI Edition, London, U.K, Chapman and Hall, 1991, ISBN 0-412-36880-3

[20] Donald A. Neamen, “Semiconductor Physics and Devices”, Third International Edition, New York, USA, Mc Graw Hill, 2003, ISBN 0-07-232107-5

[21] S. Middelhoek, S.A. Audet, and P.J. French, “Silicon Sensors”, Course Material, TU Delft, Delft, The Netherlands, 2006

[22] P.J. French and A.G.R. Evans, “Polycrystalline silicon as a strain gauge material”, J. Phys. E: Sci. Instrum. , United Kingdoms, 1986, Vol.19 No.12, 1055-1058

[23] P.J. French and A.G.R. Evans, “Piezoresistance in polysilicon and its applications to strain gauges”, Solid-State Electronics, United Kingdoms, January 1989, Vol.32 No.1, 1-10

[24] S.D. Senturia, “Microsystem design”, New York, USA, Springer, 2000, ISBN 0-7923-7246-8

[25] Chu Duc Trinh, “Sensing Microgripper”, PhD thesis, TU Delft, Delft, The Netherlands, 2007, ISBN 978-90-8559-158-0

[26] Erik V Thomsen and Jacob Richter, “Piezo Resistive MEMS Devices Theory and Applications”, DTU, Department for Micro and Nano Technology, Kgs. Lyngby , Denmark, 2005

[27] M.-H. Bao, “Micro Mechanical Transducers, Pressure Sensors, Accelerometers and Gyroscopes”, Elsevier Science, ISBN: 0 444 50558 X, 2000

[28] Rosana A. Dias, Edmond Cretu, Reinoud Wolffenbuttel and Luis A. Rocha, “Pull-in-based ug-resolution accelerometer: Characterization and noise analysis”, Sensors and Actuators A: Physical, Elsevier, 2011

[29] Chang Liu, “Foundations of MEMS”, Pearson Prentice Hall, 2006, ISBN 0-13-147286-0

[30] Brigham Young University, Resistivity & mobility calculator/graph for various doping concentrations in silicon, 2009, http://cleanroom.byu.edu/ResistivityCal.phtml, access date: February 2010

[31] Jonah A. Harley and Thomas W. Kenny, “1/f noise considerations for the design and process optimization of piezoresistive cantilevers”, Journal of Microelectromechanical Systems, June 2000, Vol.9 No.2, pp.226-235

[32] Xiaomei Yu, J. Thaysen, O. Hansen, and A. Boisen, “Optimization of sensitivity and noise in pieozoresistive cantilevers”, Journal of Applied Physics, November 2002, Vol.92 No.10, pp.6296-6301

[33] C.J.M Verhoeven, A. van Stavern, G.L.E. Monna, M.H.I. Kouwenhoven, and E. Yildiz, “Structured Electronic Design”, Course Material, TU Delft, Delft, The Netherlands, 2004, ISBN 0306487322

[34] Daniel J. Inman, “Engineering Vibration”, Prentice-Hall Inc, 2001, ISBN 0-13-726142-X

[35] SangWon Yoon, “Vibration Isolation and Shock Protection for MEMS”, PhD thesis, The University of Michigan, USA, 2009

[36] Aldo Ghisi, Fabio Fachin, Stefano Mariani, and Sarah Zerbini, “Multi-scale analysis of polysilicon mems sensors subject to accidental drops: Effect of packaging”, Microelectronics Reliability, March 2009, Vol.49 No.3, pp.340-349

[37] V. Rajaraman, Time-Based SOI Accelerometers, Technical Report (PhD Thesis Chapter), Delft University of Technology (TU Delft), The Netherlands, May-June 2011. (unpublished)

[38] V. Rajaraman, Bou Sing Hau, L.A. Rocha, R.A. Dias, R. Dekker, K.A.A. Makinwa, “A Novel SOI-MEMS “Micro-Swing” Time-Accelerometer Operating In Two Time-Based Transduction Modes For High Sensitivity And Extended Range”, Transducers 2011, Beijing, China, June 2011